Ma, X.; Blawert, C.; Hoeche, D.; Kainer, K.U.; Zheludkevich, M.L.:
Simulation assisted investigation of substrate geometry impact on PEO coating formation.
In: Surface and Coatings Technology. Vol. 350 (2018) 281 - 297.
First published online by Elsevier: July 09, 2018

DOI: 10.1016/j.surfcoat.2018.07.024
https://dx.doi.org/10.1016/j.surfcoat.2018.07.024

Simulation assisted investigation of substrate geometry impact on PEO coating formation

Xun Ma[1] *, Carsten Blawert[1], Daniel Höche[1,2], Karl U. Kainer[1], Mikhail L. Zheludkevich[1,3]

[1] Helmholtz-Zentrum Geesthacht Zentrum für Material-und Küstenforschung GmbH, Institute of Materials Research, Max-Planck-Str. 1, 21502 Geesthacht, Germany

[2] Helmut-Schmidt-University, University of the Federal Armed Forces, Faculty of Mechanical Engineering, Computational Material Design, Holstenhofweg 85, D-22043 Hamburg

[3] University of Kiel, Faculty of Engineering, Kaiserstrasse 2, 24143 Kiel, Germany

Abstract:

Plasma electrolytic oxidation (PEO) technology is widely used for coating of light metals and their alloys because of the excellent coating properties it provides and its non-line-of-sight treatment which allows forming coatings on substrates with complex geometry. However, non-uniform coating thickness and surface properties may be an issue at different locations on substrates with complex shapes. In order to understand the effect of substrate geometry on PEO coating formation and uniformity, AM50 magnesium alloy specimens with drill holes of various diameter to length ratios were coated. PEO coatings were applied on these substrates in an alkaline electrolyte at constant voltage. Phase composition, coating morphology, thickness and elements distribution were studied at different locations of the drill holes. Complementary, a 3D model describing the processing is built to simulate and to predict the effect of substrate geometry on the anodic current distribution and coating formation using finite element analyses. The model can provide useful information for predicting coating growth and uniformity towards optimized PEO process design.

Key words: PEO; geometry; simulation; coating; magnesium;

1. Introduction

Magnesium and its alloys are the lightest among the structural metallic materials, and they have outstanding features in terms of high specific strength, excellent formability, favorable ductility and high dimensional stability [1-3]. They are believed to be the engineering materials with the most exciting future wherever weight saving is at a premium [4]. However, Mg-based materials are highly susceptible to corrosion and abrasion. Plasma electrolytic oxidation (PEO) is an electrochemical surface modification technique to convert the surfaces of valve metals (Mg, Al, Ti, Zr and their alloys) into hard ceramic films with prominent wear resistance and acceptable corrosion protection [5,6]. It is similar to conventional anodizing in addition to its relatively high operating voltage, which will result in plasma discharges and dielectric breakdown of the passive film formed on the component surface in an aqueous solution [7]. The PEO coatings are typically thick and uniform. Combined PEO treatment with Mg-based materials to improve the corrosion and wear resistance, they have a great potential for application in a variety of engineering areas including aerospace, automotive, electro-communication, biomaterials etc. [8].

Compared to the other surface treatment technologies, PEO treatment is preferred for several benefits including: (a) PEO coatings are formed directly by oxidation of the metal and therefore they have good adhesion to the substrates [9]; (b) PEO treatment provides high coating growth rates to produce coating thicknesses of up to several hundreds micrometers [10]; (c) this process is easy to operate, uses nontoxic electrolyte, produces low pollution, and has no essential pretreatment step [11]; (d) PEO process is capable of non-line-of-sight treatment. The ability of non-line-of-sight treatment is of particular interest for industry, which means one can form coatings on multiple sides of samples or even on substrates with complex geometry [12]. In all the literature studying PEO process, most of them utilize samples with simplified geometries such as rectangular samples and cylinders. Only few studies have reported the influence of complex substrate geometry on PEO coatings. However, electrode geometry is one of the main factors that influence the formation of the continuous plasma envelope [13]. On the other hand, there are studies proving that even for a simplified plate sample, the anodic currents passing through the two opposite surfaces are different, which lead to divergent coating formation dynamics at different surfaces on the samples and therefore result in non-uniform coating thickness and surface properties [14,15]. Then it is reasonable to speculate that the situation on substrates with complex geometry could be even more complicated. Since uniformity is one of the main factors that influence properties of the coated samples, the PEO coatings formed on complex geometries are worth to study.

Thus, the main objective of the present paper is to study the impact of substrate geometry on PEO coatings experimentally and numerically. In this study, the substrate geometry refers to the rectangular sample of magnesium alloy AM50 with a hole of predefined diameter in the center. Samples are prepared under the same voltage mode of PEO process. Thus, the impact of different diameters on morphologies, compositions and thicknesses of PEO coatings at different locations will be discussed. The volumes inside of the holes are so small that it is difficult to observe the phenomena happening during the PEO process. Besides, the distribution of current density on the surface of the anode specimen fails to be measured through experiments, but it is worth to study because it is a determinant factor to influence the uniformity of the coating thickness and surface properties. Fortunately, modeling and simulation describing the PEO process can accomplish those tasks numerically and help to achieve better insights into the influence of substrate geometry.

2. Experimental procedures

2.1. Material and PEO treatment

AM50 magnesium alloys (4.74 wt. % Al, 0.383 wt. % Mn, 0.065 wt. % Zn, 0.063 wt. % Si, 0.002 wt. % Fe, 0.002 wt. % Cu and Mg balance) were cut into rectangular specimens (15 mm × 15 mm × 4 mm) and holes with different diameters were drilled into the centers. The diameters of the holes were 0.5 mm, 1 mm, 2 mm, 3 mm, 4 mm and 6 mm respectively. For each specimen, the inner round area around the hole was defined as the round surface, and the outer flat surface was defined as the flat surface. Before PEO treatment, the specimens were ground with silicon carbide emery papers successively from 320 grit down to 1200 grit and washed with ethanol. The electrolyte was obtained by adding KOH (1 gL^{-1}) and Na_3PO_4 (10 gL^{-1}) to deionized water, and the volume of the electrolyte used in the experiment was 2 L. A

magnetic stirrer was used to dissolve the solutes and the electrolyte temperature was maintained at 10 ± 1 ℃ by a cooling system. The conductivity of the electrolyte was 1.5 S/m, and its pH value was 13. During the PEO treatment, the AM50 substrate served as the anode and a stainless steel electrode (50 mm × 50 mm × 3 mm) served as the cathode. The anode and the cathode were located parallelly and the distance between them was adjusted to 80 mm with an accuracy of ± 1 mm. The anode surface facing the cathode was defined as the front side and the opposite surface was defined as the back side. Specimens were processed by the PEO treatment applying a constant voltage of 350 V for 10 min with a DC power supply under standard atmospheric pressure. A data acquisition system was used to record the voltage and current response. Fig.1 displays the schematic diagram of the experimental configuration and details of the definitions.

2.2. Coating characterization

The morphologies of the PEO coating, both on surfaces and in cross sections, were observed by Scanning Electron Microscopy (SEM, TESCAN Vega3 SB) in the secondary electron (SE) mode. The elemental composition and distribution of the PEO coatings were obtained by an Energy Dispersive Spectrometer (EDS). The thicknesses of oxide layers on flat coatings were determined by coating thickness gauge (Minitest 2100). The average thickness of the flat coating was determined from 3 coating samples randomly for statistical reasons. A line near the top of the hole (marked in blue in Fig.1) from the front side to the back side was selected to present the thickness distribution by cross-sectional SEM micrographs of the round coating for each sample.

3. Experimental results

The observation of discharges begins when the applied potential exceeds the breakdown potential for the PEO coatings, approx. 240 V at applied conditions. Fig.2 shows the voltage and current density transients measured from samples with different diameters of holes ranging from 0.5 mm to 6 mm at an anodically applied potential of 350 V for 10 min. In Fig.2.(a), the voltage values for the six samples increase rapidly with time and reach 350 V after 3 or 4 seconds and keeping constant value until the end of the PEO process. There are slight differences between the six samples during the voltage ramp stage. The voltage values at 1s are different. Samples with large diameters of holes have higher voltage values than those with small diameters. Furthermore, samples with larger diameters reach breakdown voltage and final voltage 350 V earlier than those with smaller diameters. There are slight differences between current density during the first 30 s as well, but then the current transients are getting closer and closer together and at the end of PEO processing time it is hard to distinguish the differences between the six samples. It is clear that the different sizes of holes have little influence on the voltage and total anodic current density evolutions. The evolution of current density for the six samples can be fitted by the same equation (1) given below and the fitted curve is in a good agreement with the experimental values.

$$j = 3.468 - \frac{3.4696 \times t^{10.98}}{1.2 + t^{0.98}} \qquad (1)$$

The relationship between current density and treatment time in Eq. (1) can be further used as modeling input data.

The characterizations of PEO coatings at two different locations, namely the outer flat surfaces and the round surfaces inside the holes, are discussed separately to determine the influence of substrate geometry on PEO coating formation. Fig.3 depicts SEM morphologies of PEO coatings chosen from the flat surfaces of AM50 substrates with different diameters of holes in a random way. All the coatings show the same typical structure of PEO coatings with micropores and projections [16]. No obvious differences are observed between those flat surfaces. Fig.4.(a) shows the elemental compositions measured by EDS on the flat surfaces of PEO coated samples with different diameters of holes. All the flat coatings are composed mainly by Mg, O, P and a small amount of Na, K and Al. The contents of these elements in different coatings have little variation and the contents for O, Mg and P are around 46 at. %, 30 at. % and 20 at. % respectively. Because of the similar morphologies and elemental contents, it is believed that the main phases in the flat coatings will be the same. According to our prior experimental results [15], the major crystalline phases in the coatings are MgO and $Mg_3(PO_4)_2$. Fig.4.(b) shows the average thickness of the flat PEO coating as a function of hole diameter with error bars showing standard deviations. The coatings on the flat surfaces have almost the same thicknesses around 17 μm. Therefore, the change of hole diameter has little influence on the morphology, composition and thickness of the flat coating.

Then characterizations of the round coatings inside the holes are discussed as follows. The morphologies of PEO coatings in Fig.5 are taken from the middle of the round surfaces of AM50 substrates. When the diameter is 0.5 mm, the image shows that there is no typical PEO coating on the round surface. Instead, the substrate is covered by loose and cracked conversion products which are similar with those formed during PEO process before reaching the breakdown potential [17]. It is possible that there are few discharges in the hole during PEO processing. The formation of discharges is influenced by the current density, the defects of local uneven electrical conductivity, the impurity level, the resistance of the coating, and the ionization coefficient of the metal oxide coating [18]. However, it is difficult to monitor the discharge behavior inside the holes by experiment. When the diameter increases to 1 mm, the round surface is covered by conversion products, rod-like particles and typical PEO structure with tiny pores and small-size projections. This morphology is similar to the flat coating treated by PEO process after reaching the breakdown potential for a short time [17]. As the diameter increases to 2 mm, no conversion products or rod-like particles can be seen in Fig.6(c), and the typical PEO coating morphology is visible covering the round surface. The micropores and projections are still small, indicating the PEO coating is thin. After the diameter reaches 3 mm, the surfaces of the round coatings show identical morphologies of typical PEO coatings. Compared with the morphologies of the flat surfaces in Fig.3, Fig.6. (d) – (f) have smaller sized projections, indicating the coating thickness on the round surfaces are thinner than that on the flat coatings.

Element composition along the length of the hole detected from the round surfaces of PEO coatings by EDS for different diameters of holes are presented in Fig.6. For each sample, ten regions with the same areas from 1 to 10 are arranged equidistantly from the front side to the

back side along the hole length. It is evident that the elemental contents are much more uniformly distributed for holes equal or larger than 2 mm. When the diameters are 0.5 and 1 mm, the contents of the main elements O, Mg and P fluctuate along with the hole length. The contents of Mg in both coatings are much lower compared to the flat coating. Compared with the flat surface composition in Fig.4, the elemental composition of 0.5 mm hole in region 1 is the same, but from region 2 to region 10, the amounts of O are much higher and the amounts of Mg and P elements are lower. It is possible that the main composition of the conversion products is $Mg(OH)_2$ which leads to the high contents of O. The content of P in 1 mm hole is higher than that in 0.5 mm hole. When the diameter ranges from 2 mm to 6 mm, the contents of Mg in the coatings remain around 30%, similar with that on the flat coatings. Mg element in the coating is derived from the substrate alloy by electrochemical reaction. The contents of Mg in the middle parts of the holes are lower than that around the edges when the hole diameters are less than 2 mm, which may indicate that the current distribution in the holes is strongly affected when the diameters are small. When the diameter is higher than 2 mm, the contents of O are around 41%, which is lower than that on the flat coatings. The decrease of O content in holes may result from the less contaminants of the coating from the air. The distribution of elements is useful for predicting the uniformity of the coating. Therefore, it suggests that the coatings inside the holes are uneven when the diameters are less than 2 mm, and above 2 mm, the coatings are more uniform.

In order to describe the distribution of coatings along the hole length, Fig.7, Fig.8 and Fig.9 show the SEM morphologies of the polished cross-sections from the front edges, the middle parts and the back edges of the round PEO coatings from 0.5 mm to 6 mm respectively. In Fig.7, when the diameter is 0.5 mm, there are thicker and thinner regions coexisting in the front edge of the hole. The thickest part is approaching 35 μm, while the thinnest part is merely 10 μm. In addition, there exists an evident crack between the coating and the substrate in Fig.7.(a), indicating the weak bonding strength between them. When the diameter is 1 mm, the coating at the front edge is still thick and the thickness is around 29 μm. From 2 mm to 6 mm, the coatings are getting thinner but more uniform, and their thicknesses are around 25 μm. In Fig.8, the middle part of the coating in 0.5 mm hole is very thin, and the thickness is around 7 μm. When the diameter is 1 mm, the coating is porous but thicker than that in the 0.5 mm hole. From 2 mm to 6 mm, the coatings have typical PEO coating structure including the inner layer, pore band and outer porous layer, and are getting much thicker and more uniform. Their average thicknesses of the inner coatings in the middle parts are around 14 μm. In Fig.9, the coating on the back edge of the 0.5 mm hole is not compact because of the missing of discharges, but its thickness is around 19 μm, higher than the other coatings with holes from 1 mm to 6 mm. But all the thicknesses of the coatings in the middle parts are smaller than that of the coatings on the edges, and the thickest coatings can be found at the front edges of the holes.

To sum up, the experimental results demonstrate that the diameters of the holes in the substrates have little effect on the growth of the flat coatings or the round coatings when the holes are large, but they can change the morphologies, compositions and thicknesses of the round coatings significantly when the diameters of the holes are smaller than 2 mm.

4. Modelling and simulation

Simulations have become an useful tool to study PEO [19, 20] or EPPo (Electrolytic plasma polishing) [21] process. A previous work has been done by our team to simulate the PEO coating formation process under constant voltage in a 2D model [19]. In order to study the PEO process at different locations of the anode, a 3D model geometry is built in Fig.10 based on the schematic representation of the experimental set-up for simulation in the present work. There are four domains in the model geometry. Domain 1 is the bulk electrolyte in the electrolyzer. Domain 2 is the cathode made of stainless steel. Domain 3 is the anode of AM50 sample with predefined diameter of hole in the center. Domain 4 is the electrolyte inside the hole. The flat surface on anode reacts with the bulk electrolyte in domain 1 and the round surface inside the hole reacts with the electrolyte in domain 4. According to our previous work [19], the main reactions occurring on Mg alloy surface in a phosphate-containing electrolyte during the PEO process are generally as following:

$$Mg \rightarrow Mg^{2+} + 2e^- \quad (2)$$

$$4OH^- \rightarrow O_2\uparrow + 2H_2O + 4e^- \quad (3)$$

$$3Mg^{2+} + 2PO_4^{3-} \rightarrow Mg_3(PO_4)_2 \quad (4)$$

$$Mg^{2+} + 2OH^- \rightarrow MgO + H_2O \quad (5)$$

However, in this study, it is possible that $Mg(OH)_2$ is formed instead of MgO inside the holes when the diameters of holes are less than 2 mm.

$$Mg^{2+} + 2OH^- \rightarrow Mg(OH)_2 + H_2O \quad (6)$$

The growth of PEO coatings mainly follows electric field-assistant mechanism [22], and the basic assumptions for the modelling are as follows:

1. The potential drops in the anode (AM50) and cathode (stainless steel) were assumed to be negligible due to their good electrical conductive properties.
2. The plasma discharges are assumed to be generated at the bottom of the pores and the length of the discharge channel is identical with the coating thickness. At each time, the discharges break down at the weak points of the coating from the bottom and leave the discharge channels as the open pores inside the coating. The oxides formed around the discharge channels will precipitate and seal most of the open pores.
3. According to Ref. [23], the total anode current *I* is consumed by two parallel processes: the current *Ic* contributing to the formation of the oxides and the current *Ip* generating oxygen and plasma. *Ip* has no contribution to the formation of the oxides.
4. The mechanism of coating growth during PEO process is predominantly electrochemical [21]. Eqs. (2) and (3) represent the electrochemical reactions during PEO process. *Ic* is the driving force of Eq. (2) and *Ip* is the driving force of Eq. (3).
5. Only crystalline phases of MgO and $Mg_3(PO_4)_2$ are considered as the composition of the PEO coating when the diameters of holes are bigger than 2 mm. Only crystalline phases of $Mg(OH)_2$ and $Mg_3(PO_4)_2$ are considered as the composition of the PEO coating inside the holes when the diameters of holes are less than 2 mm.

6. The transition time for formation of different phases in the coating is determined by the value of the potential drop across the coating which has to reach breakdown potential of 240 V. When the value of the potential drop across the coating is higher than 240 V, the phase formed in the coating is $Mg_3(PO_4)_2$. When it is less than 240 V, the phase is mainly MgO when the diameters of holes are bigger than 2 mm and the phase inside the holes are mainly $Mg(OH)_2$ when the diameters of holes are less than 2 mm.

The boundary condition at the anode is expressed by the electric potential:

$$\varphi_a = U \tag{7}$$

where U is the applied voltage.

At the cathode, the electrolyte potential is:

$$\varphi_c = 0 \tag{8}$$

The boundary condition for all the insulation walls can be expressed as:

$$-\mathbf{n} \cdot \mathbf{j} = 0 \tag{9}$$

According to the assumption, the whole current I at the anode can be described by:

$$I = I_c + I_p \tag{10}$$

The current can be described by the current density and corresponding area:

$$j \cdot S = j_c \cdot S_c + j_p \cdot S_p \tag{11}$$

where S is the area of anode, S_c is the area of oxides, S_p is the area of discharge channels, and j, j_c, j_p is the current density correspondingly.

The total current density j measured experimentally and shown in Fig. 2(b) can be expressed by Eq. (1). According to Eq. (10), it has two contributions which need to be modeled. For the current density j_c contributing to the coating formation, a modified point defect model developed by Pyun and Hong [24] can be used to describe it. In this model, it is believed that under the electric field, the movement of metal and oxygen vacancies through a passive coating make the dominant contribution to the coating growth kinetics. The final calculated dependence of the thickness on time for coatings on iron and nickel were in good agreement with those values measured experimentally [24]. Therefore, derived from their model, the theoretical equation which introduces a relationship between the current density j_c and the film thickness L is expressed by the equation below:

$$j_c = \frac{A[exp(vKL) - B \cdot exp(-vKL)]}{\exp(vKL) - 1} \tag{12}$$

Here A, B and K are constants for a certain experiment and they are determined by the polynomial least-squares procedure with the 40% of the current density evolution examined experimentally in Fig.2(b).

The porosity of a PEO coating results from the discharge channels. The current density j_p in a discharge channel is assumed constant, but the number of microplasma discharges decreases pronouncedly with time during a PEO treatment [25]. Therefore, S_p is an on-changing variable. The porosity here is described by the surface coverage of discharge channels at each moment. According to Eq. (13), the coverage ratio can be calculated at any instant of time t by:

$$P = \frac{S_p}{S} \times 100\% \tag{13}$$

The species in the electrolyte are shown in Table 1, including the corresponding parameter values of diffusion coefficients [26-28], initial concentrations and charge numbers. For each species i in the electrolyte, the general material balance [29] takes into account diffusion, migration, and convection and can be described by:

$$\frac{\delta c_i}{\delta t} + \nabla(-D_i \nabla \mathrm{c}_i - z_i u_i F c_i \nabla \varphi_i) + \mathbf{u} \nabla c_i = R_i \tag{14}$$

where c_i is the concentration, D_i is the diffusion coefficient, z_i is the charge number of the ionic species, φ_i denotes the electric potential, F is Faraday constant, R_i represents the chemical reaction rate, and $\mathbf{u}$ is the fluid flow vector. u_i is the ionic mobility. According to the Einstein relation:

$$u_i = \frac{D_i}{R_{gas} T} \tag{15}$$

where R_{gas} is the universal gas constant, T is ambient temperature.

The electric current in an electrolyte is equivalent to the transport of ionic species, so the current density in the electrolyte j_{el} can be described by Faraday's law:

$$j_{el} = F \sum z_i N_i \tag{16}$$

For the net ionic charge transport:

$$N_i = \mathbf{u} c_i - z_i u_i F c_i \nabla \varphi_i - D_i \nabla \mathrm{c}_i \tag{17}$$

Due to the electroneutrality condition, the assumption for the fluid flow vector u of the bulk electrolyte is:

$$\mathbf{u} = \mathbf{0} \tag{18}$$

Because of the stirring effect in the bulk electrolyte, the electrolyte in the holes is flowing. The velocity is so small that the flow in the holes is laminar. Therefore, the fluid flow vector of the electrolyte can be expressed by the Navier-Stokes equations [30]:

$$\begin{gathered} \rho \cdot \frac{\delta \mathbf{u}}{\delta t} + \rho \mathbf{u} \cdot \nabla \mathbf{u} = \nabla \cdot \left[-p\mathbf{I} + \eta(\nabla \mathbf{u} + (\nabla \mathbf{u})^T) - \left(\frac{2\eta}{3}\right)(\nabla \cdot \mathbf{u})\mathbf{I} \right] \\ \frac{\delta \rho}{\delta t} + \nabla \cdot (\rho \mathbf{u}) = 0 \end{gathered} \tag{19}$$

where ρ suggests density (kg/m^3), η denotes viscosity (kg/(m·s)), $\mathbf{I}$ is the identity matrix, and p is the pressure in the holes (Pa).

The boundary conditions for the holes are as follows:

$$\begin{aligned} \mathbf{u} \cdot \mathbf{n} &= v_o \qquad \text{inlet} \\ p &= p_0 \qquad \text{outlet} \\ \boldsymbol{v_0} &= w \cdot d \end{aligned} \tag{20}$$

where d is the diameter of the hole, w is a constant.

The calculated flow field serves as input to describe the convective mass transport in the holes.

According to Faraday's law, the reaction rate of the electrode surface for each species in Eqs. (5) – (6) is calculated by:

$$R_{i,m} = \frac{v_i \cdot j_c}{F \cdot n_m} \tag{21}$$

here v_i is the stoichiometric coefficient and n_m is the number of electrons exchanged in the formation reaction.

The concentration of the electrolyte at the flat surface of anode boundary is equal to the bulk concentration:

$$c_i = c_{b,i} \tag{22}$$

The electrolyte current j_{el} is then used to calculate the potential drop over the electrolyte:

$$j_{el} = -\sigma_{el} \cdot \delta E_l \tag{23}$$

The potential drop through the coating E_f including overpotential can be calculated by:

$$E_f = \varphi_a - E_l - E_a \tag{24}$$

where E_l is the potential drop through electrolyte, E_a is the equilibrium potential.

For the surface reaction, we assume that all the magnesium ions participate in the formation of PEO coating. Here only a one-dimensional growth of PEO coating in the perpendicular direction of the surface is considered. The PEO coating includes the growth of barrier layer at the initial stage and the growth of the outer layer at the later stage. When the potential drop over the coating is lower than 240 V, the main phase of the barrier layer is MgO as the diameter of a hole is bigger than 2 mm, and the main phase of the barrier layer is $Mg(OH)_2$ as the diameter of the hole is less than 2 mm. The the growth rates of MgO and $Mg(OH)_2$ are as follows:

$$R_{MgO} = R_{Mg^{2+}} \tag{25}$$

$$r_{MgO} = \frac{R_{MgO} \cdot M_{MgO}}{\rho_{MgO}} \tag{26}$$

$$r_{MgOH} = \frac{R_{MgO} \cdot M_{MgOH}}{\rho_{MgOH}} \tag{27}$$

where M_{MgO} is the molar mass and ρ_{MgO} is the density of MgO phase in the coating, and M_{MgOH} is the molar mass and ρ_{MgOH} is the density of $Mg(OH)_2$ phase.

At the later stage, the reaction rate of the main phase $Mg_3(PO_4)_2$ is calculated by:

$$R_{MgP} = \frac{R_{Mg^{2+}}}{3} \tag{28}$$

Accordingly, the growth rate for the outer layer is determined by the $Mg_3(PO_4)_2$ phase and the porosity (P) when the potential drop over the coating is higher than 240 V:

$$r_{MgP} = \frac{R_{MgP} \cdot M_{Mg3(PO4)2}}{(1-P) \cdot \rho_{Mg3(PO4)2}} \tag{29}$$

where $M_{Mg3(PO4)2}$ is the molar mass and $\rho_{Mg3(PO4)2}$ is the density of $Mg_3(PO_4)_2$ phase in the coating.

However, the volume of the electrolyte inside the hole is limited, especially when the size of the hole is small. The changes of the ions in the electrolyte in domain 4 may result in different growth rate. Therefore, the solubility products and ion products of $Mg(OH)_2$ and $Mg_3(PO_4)_2$ have to be considered.

$$Q_{MgP} = {c_{Mg2+}}^3 \cdot {c_{PO3-}}^2 \tag{30}$$

$$Q_{MgOH} = c_{Mg2+} \cdot {c_{OH-}}^2 \tag{31}$$

c_{Mg2+}, c_{PO3-} and c_{OH-} are the concentrations of Mg^{2+}, PO_4^{3-}, and OH^- respectively. When the ion products of Q_{MgOH} and Q_{MgP} are lower than their solubility product $K_{sp(MgOH)}$ *and* $K_{sp(MgP)}$, magnesium oxide, magnesium hydroxide and magnesium phosphate are not able to form. The growth rate of each phase is determined as following:

$$v_{Mgo} = \begin{cases} 0 \left(Q_{MgOH} < K_{sp(MgOH)}\right) \\ r_{MgO}\left(Q_{MgOH} \gg K_{sp(MgOH)}\right) \end{cases} \tag{32}$$

$$v_{MgoH} = \begin{cases} 0 \left(Q_{MgOH} < K_{sp(MgOH)}\right) \\ r_{MgOH}\left(Q_{MgOH} \gg K_{sp(MgOH)}\right) \end{cases} \tag{33}$$

$$v_{Mgpo} = \begin{cases} 0 \left(Q_{MgP} < K_{sp(MgP)}\right) \\ r_{Mgpo}\left(Q_{MgP} \gg K_{sp(MgP)}\right) \end{cases} \tag{34}$$

where $K_{sp(MgOH)}$ and $K_{sp(MgP)}$ are the solubility products of $Mg(OH)_2$ and $Mg_3(PO_4)_2$ respectively.

The initial pH value of the electrolyte is in the passive region of AM50 magnesium alloy, so a natural passive film would be formed when the magnesium electrode is immersed in the electrolyte [20]. In this manner, it is assumed that the substrate has a thin magnesium oxide layer L_0, and the total coating thickness L when the diameters of holes are larger than 2 mm can be calculated by:

$$L = L_0 + \int_0^{t0} v_{MgO}\, \mathrm{d}t + \int_{t0}^{t} v_{Mgpo}\, \mathrm{d}t \tag{35}$$

When the diameters of holes are less than 2 mm, the total coating thickness L inside the holes can be calculated by:

$$L = L_0 + \int_0^{t0} v_{mgoH}\,\mathrm{d}t + \int_{t0}^{t} v_{mgpo}\,\mathrm{d}t \qquad (36)$$

where t_0 is the time when the potential drop reaches 240 V.
Table 2 summarizes the most important parameters being used for the computation. Combining all the parameters in Table 1 and Table 2, with the respective boundary conditions, the model is solved numerically via finite element method for time-dependent study in 10 min with a time stepping of 1 s using the commercial software COMSOL Multiphysics (version 4.4).

5. Simulation results

The evolution of the average current density with time on the flat surfaces (a) and the round surfaces (b) are presented in Fig.11. In Fig.11(a), the simulated values of average current density on flat surfaces of different geometries show the identical evolution with time. They decrease with time in a similar way with the evolution of the total current density in Fig.2 and the sizes of the holes do not have much influence on them. In Fig.11(b), on the round surfaces, the evolutions of the average current density with diameters ranging from 2 mm to 6 mm behave analogously and their values are lower than that on the flat surfaces. However, the average current density on the round surfaces in the holes with diameters of 0.5 mm and 1 mm change with time differently. Before they begin to decrease similarly with others, there is a time interval approx. 100 s and 11 s for holes with diameters of 0.5 mm and 1 mm separately that they decrease gradually with time in a linear way.

The dependence of the average potential drop including overpotential through both the flat (a) and the round (b) coating layers on the PEO processing time for samples with the diameters of holes ranging from 0.5 mm to 6 mm are presented in Fig.12. The potential drop through the coating is calculated according to Eq. (23). On the flat surfaces, it increases over time rapidly from 250 V at 1 s and reaches to approx. 350 V at the later stage of the processing time. The evolution is identical for each sample with different hole size, indicating the same growth rate of coatings. On the round surfaces, the potential drop also increases with time, but the increasing rate for each sample is different. The smaller the diameter is, the slower the increasing rate is. The potential drop through the coating is related to the discharges. When the potential difference is higher than the breakdown voltage 240, the discharges are possible to emerge. Therefore, for the coatings inside the holes, it takes at least 100 seconds for 0.5 mm sample, and 11 seconds for 1 mm sample and less than 4 seconds for samples from 2 mm to 6 mm to generate plasma. But for coatings on the flat surfaces, after 1 s, plasma discharges start, which is in accordance with the experimental observation.

Fig.13 shows the simulated changes of average concentrations of OH^- and PO_4^{3-} both in the bulk electrolyte (a and b) and the electrolyte inside the holes (c and d) over time. The decrease of PO_4^{3-} concentration is a result of the formation of $Mg_3(PO_4)_2$ phase in the coating. OH^- is consumed by both oxygen release and the formation of MgO or $Mg(OH)_2$ in the coating. It is clear that the changing hole size in the range of 0.5 mm to 6 mm does not affect the concentrations of PO_4^{3-} and OH^- in the bulk electrolyte, and after 10 min PEO processing, the changes of PO_4^{3-} and OH^- in the bulk electrolyte are inconspicuous. However, in the holes, the concentrations of OH^- and PO_4^{3-} show quite different evolution compared to the bulk

electrolyte. The initial concentration of OH^- is 29.2 mol/m^3 for all the conditions. Then in the first second, the concentration of OH^- decreases rapidly. For the holes with sizes of 0.5 mm, 1 mm, and 2 mm, the concentration of OH^- decreases almost to 0, which means the electrolyte is limited. Then with increasing time, the concentration of OH^- increases gradually due to the supplement of electrolyte from the container. It takes much longer time to recover the concentration of OH^- when the hole size is smaller. For the smallest hole with 0.5 mm diameter, it takes almost 100 s, but for the 6 mm hole, it takes less than 1 s. The final concentration values of OH^- in the holes are lower than that in the bulk electrolyte and the smaller the hole is the lower the concentration is. Fig.13(d) shows the evolution of the concentration of PO_4^{3-} in the holes. The initial concentration of PO_4^{3-} is 61 mol/m^3. Different from the evolution of OH^-, the concentration of PO_4^{3-} keeps constant for a while before it begins to decrease because the PO_4^{3-} is consumed by formation of $Mg_3(PO_4)_2$ at the later stage. The time interval is determined by the potential drop reaching breakdown potential and it decreases with increasing hole size. After that the concentration decrease rapidly due to the high reaction rate of $Mg_3(PO_4)_2$ and then increase because of the decreasing reaction rate and the supplement from the bulk electrolyte. The concentrations of PO_4^{3-} in the hole with diameter of 0.5 mm decreases to approx. 0 and remain for several seconds, indicating the shortage of ions in the electrolyte may restrict the coating formation reaction.

Fig.14 displays the evolution of average coating thickness with time on the flat surfaces (a) and round surfaces (b) of samples with diameters of holes ranging from 0.5 mm to 6 mm. As expected, the coatings show the same evolution of thickness on the flat surfaces. The average coating thickness increases gradually with time and the final thickness is around 16.5 μm for each sample, which is in agreement with the experimental values. On the round surfaces, the evolution of the coating thickness for samples with holes larger than 2 mm are similar with that on flat surfaces, and their final coating thickness are around 14.5 μm. When the holes are smaller than 1 mm, the evolution of average coating thickness is significantly different. The thickness increases linearly with time by a low growth rate in the first period of time that lasts for approx. 100 s and 10 s for 0.5 mm and 1 mm samples respectively, and then it increases gradually in the same manner of the outer coating thickness till the end of the processing time. The final coating thicknesses of 0.5 mm and 1 mm samples are 12.7 μm and 13.4 μm respectively.

Fig.15 illustrates how the geometry affect the pore coverage ratio at the flat surfaces (a) and the round surfaces (b) with increasing time. The simulation results show that the pore coverage ratio on flat surfaces is a little bit higher as compared to the round surfaces. The changing geometry does not alter the evolution of the pores on flat surfaces and round surfaces with holes larger than 2 mm. The pore coverage ratio drops down rapidly at the early stage of the PEO processing and then increases slowly till the end. When the diameters of holes are 0.5 mm and 1 mm, there is no discharges generated at the initial stage because breakdown potential is not reached. After 200 s and 50 s for samples with 0.5 mm and 1 mm holes respectively, the pore coverage ratio increases gradually with time. Nevertheless, the values are less than 0.3 %, so the plasma discharges in both holes are very rare.

Fig.16 presents the simulation results of concentration distribution of OH^- along the length of different holes at different times. The concentration of OH^- in the middle parts of the holes are lower compared to the edge parts which can be attributed to the diffusion, convection and migration of ions in the bulk electrolyte from both edges to the center of the holes. The concentration in the smallest hole is the lowest, and with increasing hole size, the concentration gets higher and higher. At the first second, the concentration reaches to approx. 0 mol/m^3 inside 0.5 mm hole, and it takes more than 90 s to recover back. In 1 mm hole it takes 10 s, and in 2 mm and 3 mm hole, it takes less than 2 s to recover back to more than 0 mol/m^3. For 4 mm and 6 mm holes, the concentration remains higher than 8 mol/m^3. The values of ion concentrations in the small holes indicate that the formation of PEO coatings on the round surfaces with diameters of holes below 2 mm might be delayed because of shortage of the electrolyte.

In order to discover how the current distributes along the length of the round surface, the same position of the line shown in blue in Fig.1 at the top of the hole is selected from the front side to the back side. The simulation results of current distribution for different holes at different times are shown in Fig.17. For each sample, the current density decreases firstly from the front side and then increases a little bit at the back side at any moment. When the diameter is 0.5 mm, the current density decreases rapidly near the front edge but keeps stable in the middle part. As the diameter reaches to 1 mm, the decrease of current density at the front edge becomes less steeper. From 2 mm to 6 mm, the current density decreases gradually over the length and the distribution of current density shows no significant difference between those samples. Moreover, the highest value of current density is found for the front side of 0.5 mm hole.

Since it is difficult to measure the average coating thickness inside the holes statistically by experiment, the line near the place where we show the cross-sections in Fig.7, Fig.8 and Fig.9 is selected to show the distribution of coating thickness along the length of the hole from the front side to the back side for each sample. The simulation results at different times are shown in Fig.18. For the round coating inside the hole with 0.5 mm diameter, there is a time interval around 100 s during which the coating formation is slowed down, leading to the thin coating in most of the hole. The same situation happens to the hole with 1 mm diameter, and the time interval is at least 10 s. But both coatings grow quickly after 120 s and 30 s respectively. At the end of processing time, the distribution of thickness for 0.5 mm is obviously different from the others with rapid decrease of coating thickness at both edges and the quite thin and uniform thickness in the middle of the coating, and the highest value at the front side is approx. 36 μm and the lowest value is approx. 8 μm in the middle part. The final coating thickness of the 1 mm sample show the similar distribution with that of the 0.5 mm sample. The coating thickness at both edges are lower than that of 0.5 mm sample, and the coating thickness in the middle is around 12 μm, thicker than that of the 0.5 mm hole.

For the other holes with diameters from 2 mm to 6 mm, the time intervals are in the range of 2 to 4 s. The thickness at each point increases with time but the growth rate decreases from the front side to the back side gradually for each sample. After 10 min, the distributions of coating thickness between those samples do not have much difference, with around 22 μm at the front

side and around 15 μm in the middle part. At the front edge of each hole, the current density is the highest, and the supplement of the electrolyte is faster than in the middle part, so the coating is much thicker at the end than that in the middle part. The simulation results show that the current density at the front edge of 0.5 mm hole is the highest, hence the coating at this part is correspondingly the thickest. In comparison, the simulation results are in good agreement with the experimental results of coating thickness distribution from Fig.7 to Fig.9.

6. Discussion

In the present study, the geometry of the substrate is separated mainly into two parts, the flat surface and the round surface. The coating growth on both the flat and round surfaces result from the reactions of the substrate with the electrolyte in domain 1 and domain 4 respectively under constant voltage mode. The experimentally measured conductivity in bulk electrolyte after the 10 min PEO processing is almost the same as the one measured before, and the pH values decrease only by 0.05 after 10 min. Therefore, in the modelling, we assume that the magnesium ions generated on the flat surface will react completely with the bulk electrolyte. Over the total PEO processing time, the simulated concentrations of both OH^- and PO_4^{3-} ions in bulk electrolyte show little changes after 10 min. The changing sizes of the holes have barely influence on the simulation results of the average current density and the potential drop over the coating on the flat surfaces, which generates the same growth rate of the PEO coatings. Therefore, the assumptions of the mechanism on the flat surface hold true for the calculation of current distribution and coating thickness, and the coating characterization and the measured coating thickness from the experiment on flat surfaces are identical after the same PEO processing even though the sizes of the holes change from 0.5 mm to 6 mm.

However, the coatings inside the holes are affected by the changing size of the holes. The main factors that influence the quality of the formed PEO coating are the processing parameters, such as the applied potential, the applied current density, the treatment time, the substrate properties, electrode geometry, nature and additives of the electrolyte, and flow dynamics [31]. In this study, the changing geometry leads to different volumes of electrolyte inside the holes. When the diameters range from 0.5 mm and 1 mm, due to their small amount of electrolyte inside the holes, the evolutions of the concentration of ions inside the holes, the average current density, the potential drop, the coating thickness and the pore coverage ratio differ greatly from those with hole diameters more than 2 mm. At the initial stage, the formation of the oxide products demands a large amount of OH^- in the electrolyte. The simulation results show that the amount of OH^- in the middle parts of the small holes decreases rapidly to 0 especially when the size of the holes are small, indicating that the electrolyte inside the holes is not enough for the coating growth on the round surfaces. The deficiency of electrolyte restrains the growth of coatings and thus slows down the decrease of current density and the increase of voltage drop across the coatings. Before the voltage drop reaches 240 V, no plasma is formed and the process is similar to conventional anodization. The duration of conventional anodization for coatings inside the 0.5 mm and 1 mm holes are about 90 s and 11 s respectively, which are much longer than those inside the holes with diameters more than 2 mm. The properties of the electrolyte in holes may change sharply, pH for example. The consumption of OH^- may lead to acidification of the electrolyte, then in such a condition, magnesium hydroxide and magnesium phosphate can not form, and most of

the substrate may dissolve in the electrolyte in the form of Mg^{2+} instead. Therefore, the Mg contents of the ceramic coating in the middle parts of the small holes with diameters of 0.5 mm and 1 mm are lower than that of the other coatings, and the formation mechanism for the coatings is different from what we have observed from experiments on flat surfaces. Then after the potential drop reaches 240 V, plasma discharges associated oxidation enables the fast growth of PEO coatings and leads to a rapid decrease of current density and increase of potential drop. Even though there are plasma discharges generated at the later stage of the PEO processing inside the smallest hole, the shorter duration and low ratio of the discharges can barely condense the coating, leading to loose conversion products on the surfaces of the holes. The plasma discharge in the hole with 1 mm diameter lasts longer and its ratio is higher as compared to the smallest hole. Thus, it is possible to condense some conversion products. The coating is a mixture of some typical PEO structures and conversion products. The final coating thickness is determined by both the concentration of the ions and the current distribution inside the holes. The current density and the concentration of ions at the edges are higher compared to the middle, resulting in thick coatings at both edges and thin coatings in the middle of the holes.

For samples with diameters ranging from 2 mm to 6 mm, their relatively large volumes of electrolyte inside the holes guarantee a fast supply of the ions for the chemical reactions. Even though the concentrations of OH^- in the middle of the holes with diameters of 2 mm and 3 mm decrease to approx. 0 in the first second, they recover in less than 2 s. Therefore, the PEO coatings still grow fast from the initial stage, and the values of current density decreases and the values of voltage drop over the PEO film increases rapidly from the beginning of PEO treatment, which complies with the typical features of current and voltage evolution under constant voltage mode. The distribution of their final coating thicknesses is determined mainly by the distribution of the current density. Also, the coating thickness on round surface within 2 mm and 3 mm holes are thinner than that with larger holes due to the postponement of coating growth in the first seconds by the shortage of electrolyte.

From the results above, it is concluded that when the electrolyte is sufficient, current density is the main factor that influence the coating growth, but when the electrolyte is deficient, the concentration of ions controls the growth of PEO coating.

7. Conclusion

1. In this study, the substrate geometry refers to rectangular sample of magnesium alloy AM50 with a hole of predefined diameter in the center. The experimental results demonstrate that the size of the holes barely has influence on the flat coatings, but it does have a significant influence on the inner round coatings when the diameters of the holes are small. The coatings inside the holes are thinner than their corresponding flat coatings, especially when the diameter is less than 2 mm. The morphology, composition of the inner coatings inside the holes with diameters less than 2 mm differ from the flat coatings greatly. The coatings are loose and have only few typical PEO coating features, and most of the coatings are composed of conversion products. The contents of Mg element in those coatings are lower compared to coatings with larger diameters of holes. The distribution of the elements along the length of the holes are fluctuant and thus the distribution of the coating thicknesses are not uniform. The

coatings at the edges are very thick while the coatings in the middle of the hole length are very thin.

2. A 3-D model has been applied for calculation of the coating thickness on complex substrate geometry. Modeling and simulation reproduce the PEO process on both outer flat surface and inner round surface of magnesium AM50 alloy reasonably well. The simulation results show that the size of holes has little influence on the flat coatings which is in accordance with the experimental results, but inside the holes, the round surfaces are strongly affected especially when the diameters of the holes are smaller than 2 mm. In addition, the simulation results reveal that the shortage of electrolyte is the main reason that affects the growth of the coating and thus the composition and morphology of the coating inside the holes, and the final simulation results of the coating thickness are in good agreement with experimental values.

Therefore, we come to the conclusion that substrate geometry indeed has impact on PEO coating growth under constant voltage mode because of the different current distribution and evolution as well as the constraint of the electrolyte at different locations, and substrates are suggested to avoid having open holes with diameters less than 2 mm. Meanwhile, modeling and simulation have been proved to be a useful tool to help understand and predict the PEO process reasonably.

Acknowledgements

The authors are grateful for funding of the award of fellowship from China Scholarship Council to Xun Ma and the assistance of Mr. Zahid M. Mir, Mr. Ulrich Burmester, Mr. Volker Heitmann and Mr. Hailin Tseng during the course of this work.

Reference

[1] H. Somekawa, A. Kinoshita, K. Washio, A. Kato, *Enhancement of room temperature stretch formability via grain boundary sliding in magnesium alloy*. Mater. Sci. Eng. A, 676 (2016), pp. 427-433.

[2] Y. Liu, X. Yin, J. Zhang, S. Yu, Z. Han, L. Ren, A electro-deposition process for fabrication of biomimetic super-hydrophobic surface and its corrosion resistance on magnesium alloy. Electrochimica Acta, 125 (2014), pp. 395-403.

[3] H.Y. Wang, W. Wang, M. Zha, N. Zheng, Z.H. Gu, D. Li, Influence of the amount of KBF4 on the morphology of Mg2Si in Mg-5Si alloys. Mater. Chem. Phys., 108 (2008), pp. 353-358.

[4] A. Kuhn, *Plasma anodizing of magnesium alloys*. *Metal Finishing*, 101 (2003), pp. 44-50.

[5] A. L. Yerokhin, X. Nie, A. Leyland, A. Matthews, S. J. Dowey, *Plasma electrolysis for surface engineering*. Surf. Coat. Technol., 122 (1999), pp. 73-93.

[6] X. Lu, C. Blawert, D. Tolnai, T. Subroto, K. U. Kainer, T. Zhang, et al. *3D Reconstruction of Plasma Electrolytic Oxidation Coatings on Mg Alloy via Synchrotron Radiation Tomography*. Corros. Sci., 139 (2018), pp. 395-402.

[7] E. Cakmak, K. C. Tekin, U. Malayoglu, S. Shrestha, *The effect of substrate composition on the electrochemical and mechanical properties of PEO coatings on Mg alloys*. Surf. Coat. Technol., 204 (2010), pp. 1305-1313.

[8] H. N. Vatan, R. Ebrahimi-kahrizsangi, M. Kasiri-asgarani, *Structural, tribological and electrochemical behavior of SiC nanocomposite oxide coatings fabricated by plasma electrolytic oxidation (PEO) on AZ31 magnesium alloy*. J. Alloys. Compd., 683 (2016), pp. 241-255.

[9] X. Ma, S. Zhu, L. Wang, C. Ji, C. Ren, S. Guan, *Synthesis and properties of a bio-composite coating formed on magnesium alloy by one-step method of micro-arc oxidation.* J. Alloys. Compd., 590 (2014) , pp. 247-253.

[10] A.G. Rakoch, A.A. Gladkova, Z. Linn, D.M. Strekalina, *The evidence of cathodic micro-discharges during plasma electrolytic oxidation of light metallic alloys and micro-discharge intensity depending on pH of the electrolyte.* Surf. Coat. Technol., 269 (2015), pp. 138-144.

[11] L. Chang, *Growth regularity of ceramic coating on magnesium alloy by plasma electrolytic oxidation.* J. Alloys. Compd., *468* (2009), pp. 462-465.

[12] E.V. Parfenov, A. Yerokhin, R.R. Nevyantseva, M.V. Gorbatkov, C.J. Liang, A. Matthews, Towards smart electrolytic plasma technologies: An overview of methodological approaches to process modelling, Surf. Coat. Technol. 269 (2015) 2–22.

[13] P. Gupta, G. Tenhundfeld, E. O. Daigle, D. Ryabkov, *Electrolytic plasma technology: science and engineering—an overview*. Surf. Coat. Technol., 201(2007), pp. 8746-8760.

[14] C.B. Wei, X.B. Tian, S.Q. Yang, X.B. Wang, Ricky K.Y. Fu, Paul K. Chu, *Anode current effects in plasma electrolytic oxidation.* Surf. Coat. Technol., 201 (2007), pp. 5021-5024.

[15] X. Ma, C. Blawert, D. Höche, M. L. Zheludkevich, K. U. Kainer, *Investigation of electrode distance impact on PEO coating formation assisted by simulation*. Appl. Surf. Sci., 388 (2016), pp. 304-312.

[16] Y. Cheng, Z. Peng, X. Wu, J. Cao, P. Skeldon, G. E. Thompson, *A comparison of plasma electrolytic oxidation of Ti-6Al-4V and Zircaloy-2 alloys in a silicate-hexametaphosphate electrolyte.* Electrochim. Acta, 165 (2015), pp. 301-313.

[17] X. Lu, C. Blawert, K. U. Kainer, M. L. Zheludkevich, *Investigation of the formation mechanisms of plasma electrolytic oxidation coatings on Mg alloy AM50 using particles*. Electrochim. Acta, 196 (2016), pp. 680-691.

[18] T. Mi, B. Jiang, Z. Liu, L. Fan, *Plasma formation mechanism of microarc oxidation*, Electrochim. Acta, 123 (2014), pp. 369–377.

[19] X. Ma, C. Blawert, D. Höche, K. U. Kainer, M. L. Zheludkevich, *A model describing the growth of a PEO coating on AM50 Mg alloy under constant voltage mode*. Electrochim. Acta, 251 (2017), pp. 461–474.

[20] J.P. Caire, F. Dalard, W.S. Minko, Modeling the plasma electrolytic oxidation of aluminium and magnesium alloys, ECS Trans. 2 (2007) 1–21.

[21] E. V. Parfenov, R. G. Farrakhov, V. R. Mukaeva, A. V. Gusarov, R. R. Nevyantseva, A. Yerokhin, *Electric field effect on surface layer removal during electrolytic plasma polishing*. Surf. Coat. Technol., 307, (2016), pp. 1329-1340.

[22] H. Duan, C. Yan, F. Wang, *Growth process of plasma electrolytic oxidation films formed on magnesium alloy AZ91D in silicate solution*. Electrochim. Acta, 52 (2007), pp. 5002-5009.

[23] A. L. Yerokhin, V. V. Lyubimov, R. V. Ashitkov, *Phase formation in ceramic coatings during plasma electrolytic oxidation of aluminium alloys*. Ceram. Int., 24 (1998), pp. 1-6.

[24] S. I. Pyun, M. H. Hong, *A model describing the growth kinetics of passivating oxide film prepared under potentiostatic conditions*. Electrochim. Acta, 37 (1992), pp. 327-332.

[25] A. G. Rakoch, V. V. Khokhlov, V. A. Bautin, N. A. Lebedeva, Y. V. Magurova, I. V. Bardin, *Model concepts on the mechanism of microarc oxidation of metal materials and the control over this process.* Prot. met., 42 (2006), pp. 158-169.

[26] D. Höche, *Simulation of Corrosion Product Deposit Layer Growth on Bare Magnesium Galvanically Coupled to Aluminum*. J. Electrochem. Soc., 162 (2015), pp. 1-11.
[27] M. D. Krom, R. A. Berner, *The diffusion coefficients of sulfate, ammonium, and phosphate ions in anoxic marine sediments*. Limnol. Oceanogr., 25 (1980), pp. 327-337.
[28] A. M. Friedman, J. W. Kennedy, *The Self-diffusion Coefficients of Potassium, Cesium, Iodide and Chloride Ions in Aqueous Solutions1*. J. Am. Chem. Soc., 77 (1955), pp. 4499-4501.
[29] R. Taylor, R. Krishna, Multicomponent mass transfer. John Wiley & Sons. 1993.
[30] R. Aris, Vectors, tensors and the basic equations of fluid mechanics. Courier Corporation, 2012.
[31] J. Garbarz-Olivier, C. Guilpin, The origin of the electrode effect in various electrolytes, J. Electroanal. Chem., 91 (1978), pp. 79-91.

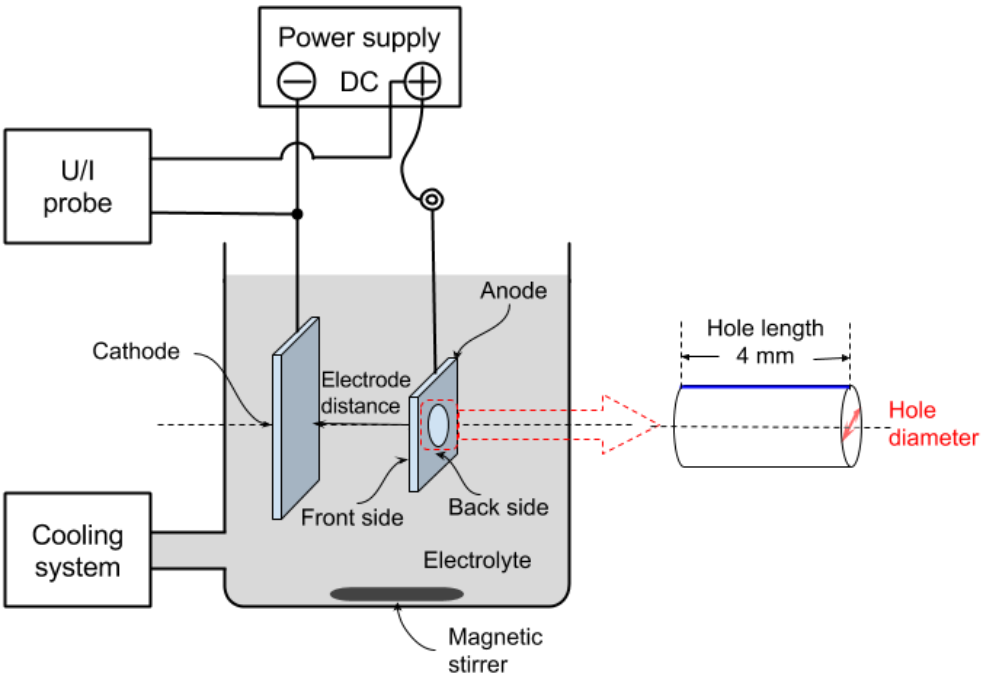

Fig.1 Schematic diagram of the experimental set-up. The predefined diameters of holes in the center of AM50 anode range from 0.5 mm to 6 mm.

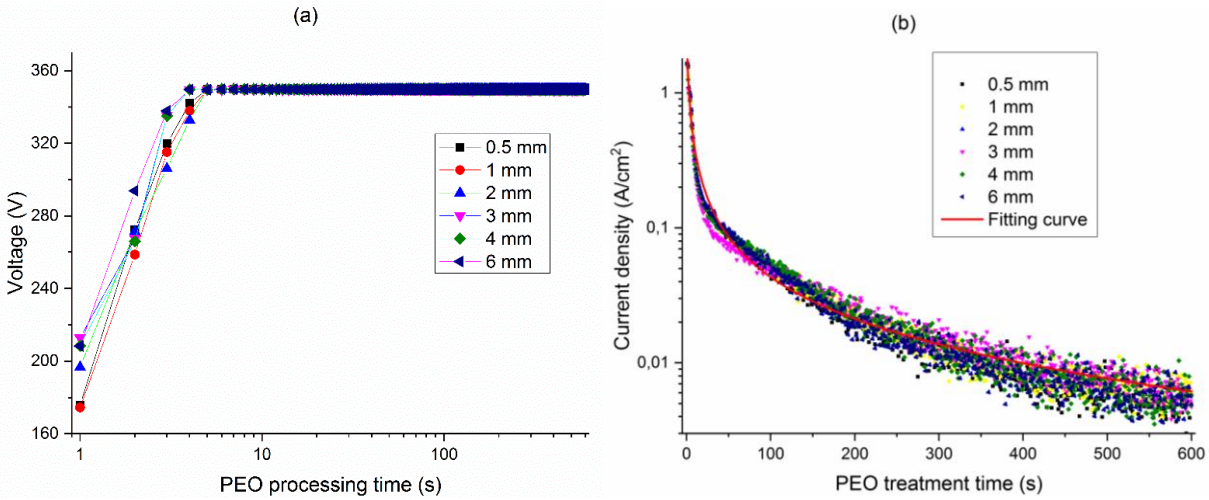

Fig.2 Voltage (a) and current density (b) transients measured from samples with different diameters of holes ranging from 0.5 mm to 6 mm at an anodic applied potential of 350V in 10 min and the corresponding fitting curve for current density.

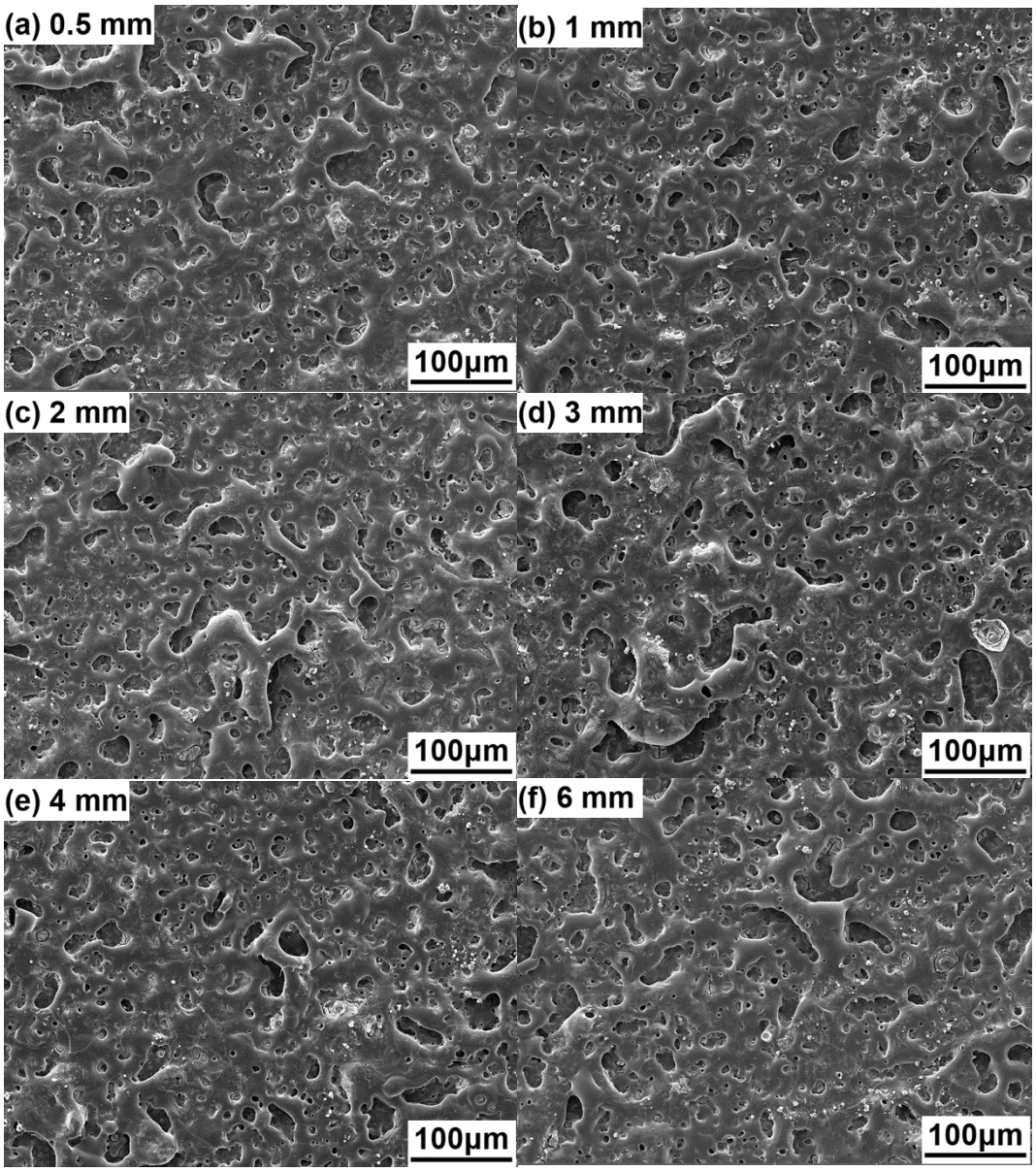

Fig.3 SEM morphologies of PEO coatings on the flat surfaces of AM50 substrates with different diameters of holes.

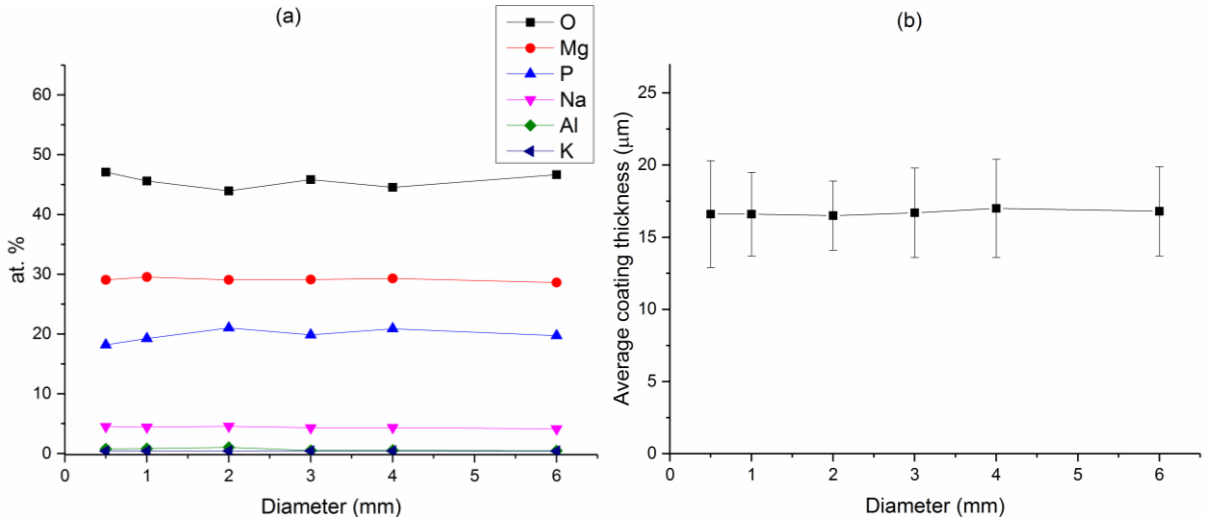

Fig.4 (a) Elemental composition detected by EDS on the flat surfaces of PEO coated samples with different diameters of holes; (b) Average thickness of PEO coating on flat surface with the error bar showing standard deviations as a function of hole diameter.

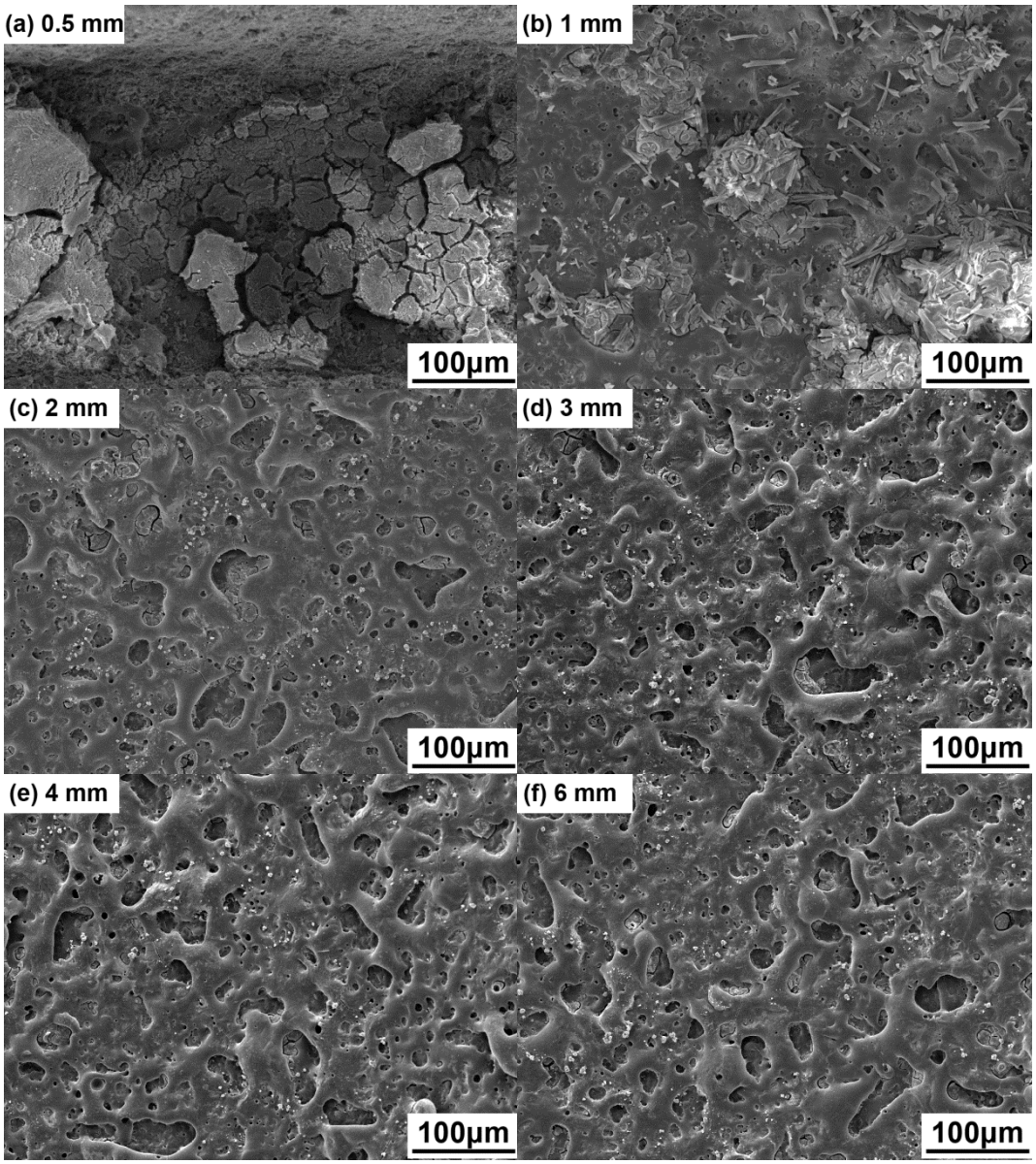

Fig.5 SEM morphologies of PEO coatings on the round surfaces of AM50 substrates with different diameters of holes.

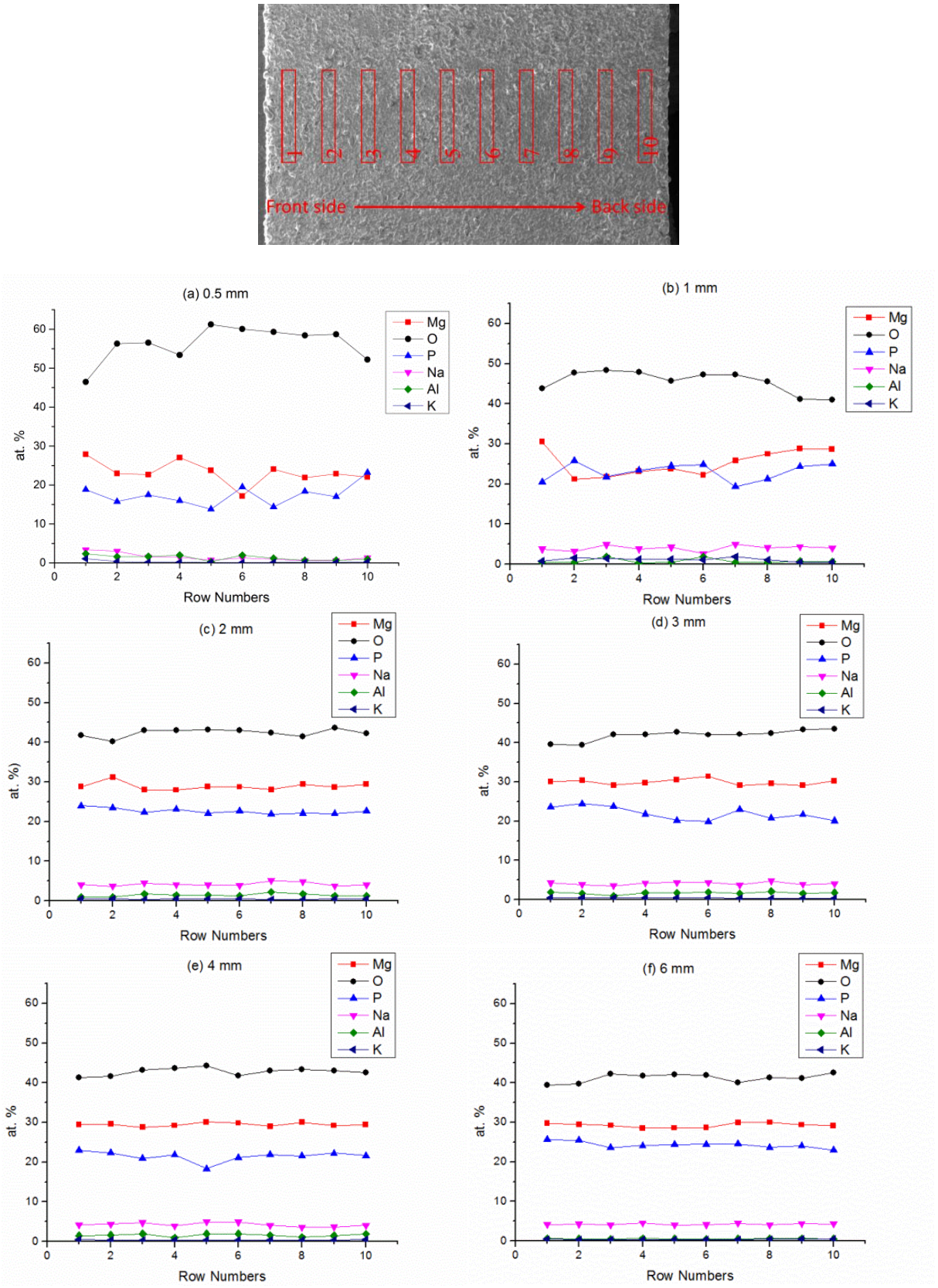

Fig.6 Elements composition along the hole length detected from the round surfaces of PEO coatings by EDS for different diameters of holes.

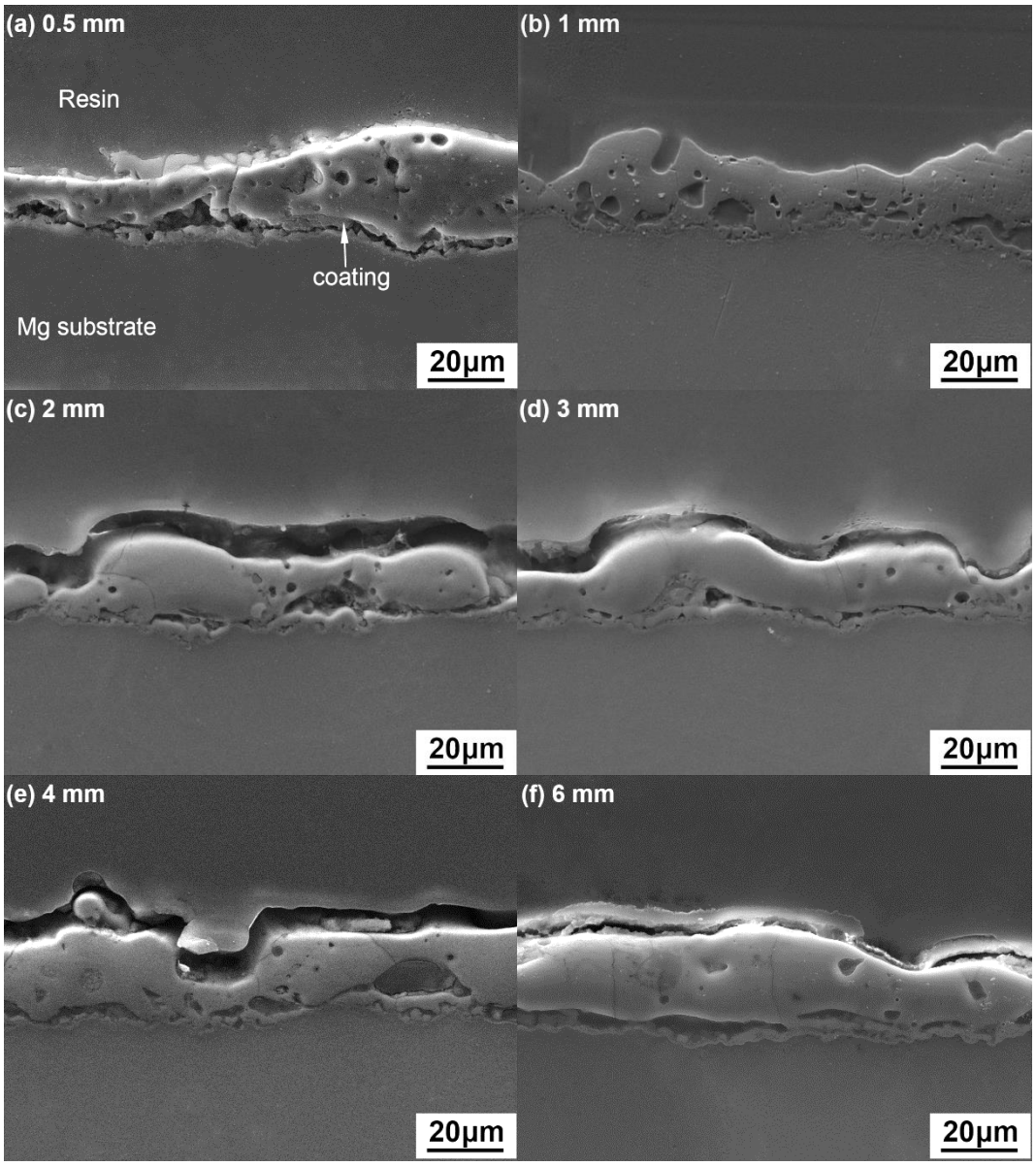

Fig.7 SEM morphologies of the polished cross-sections from the front edge of the round PEO coatings.

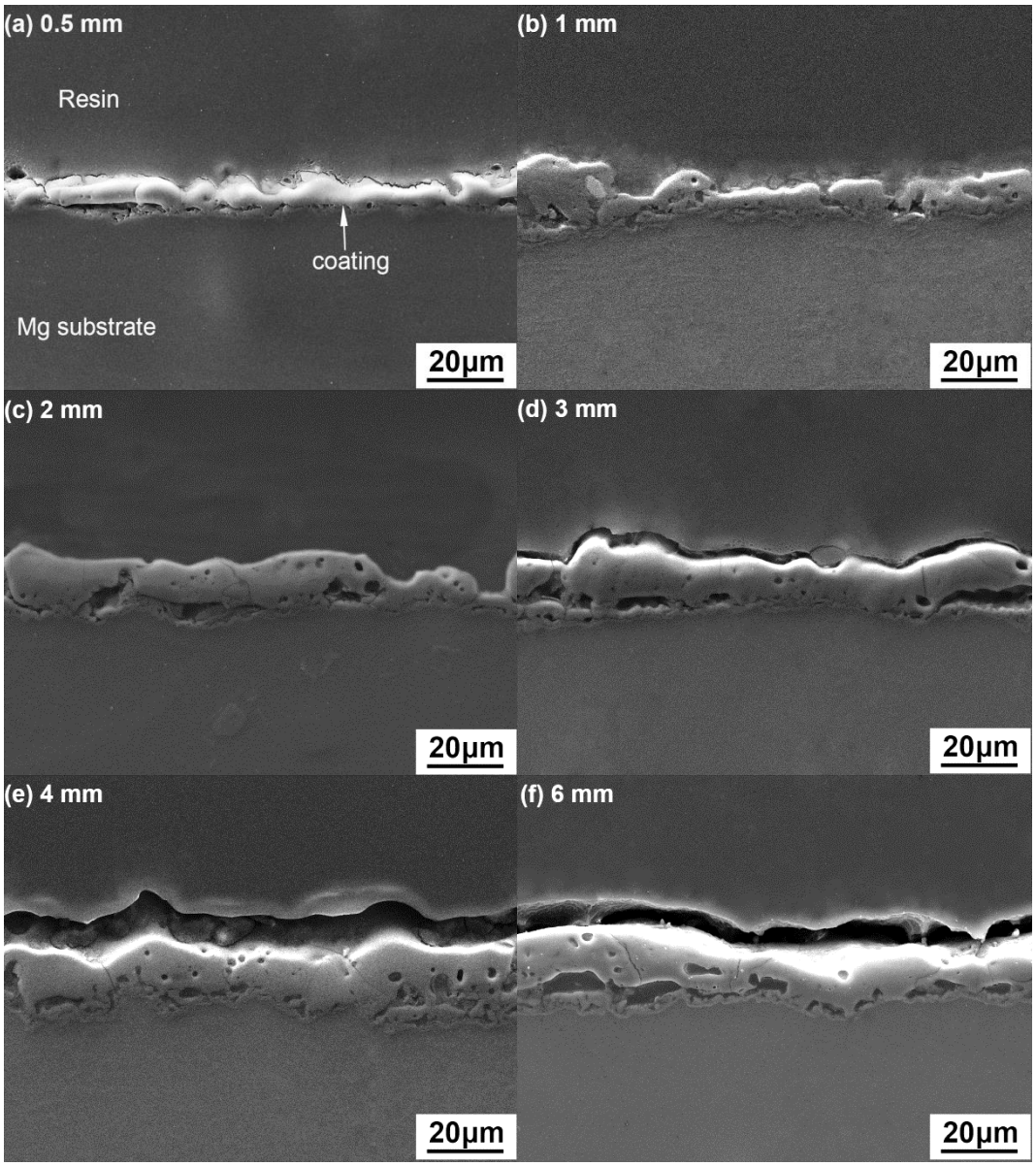

Fig.8 SEM morphologies of the polished cross-sections from the middle parts of the round PEO coatings.

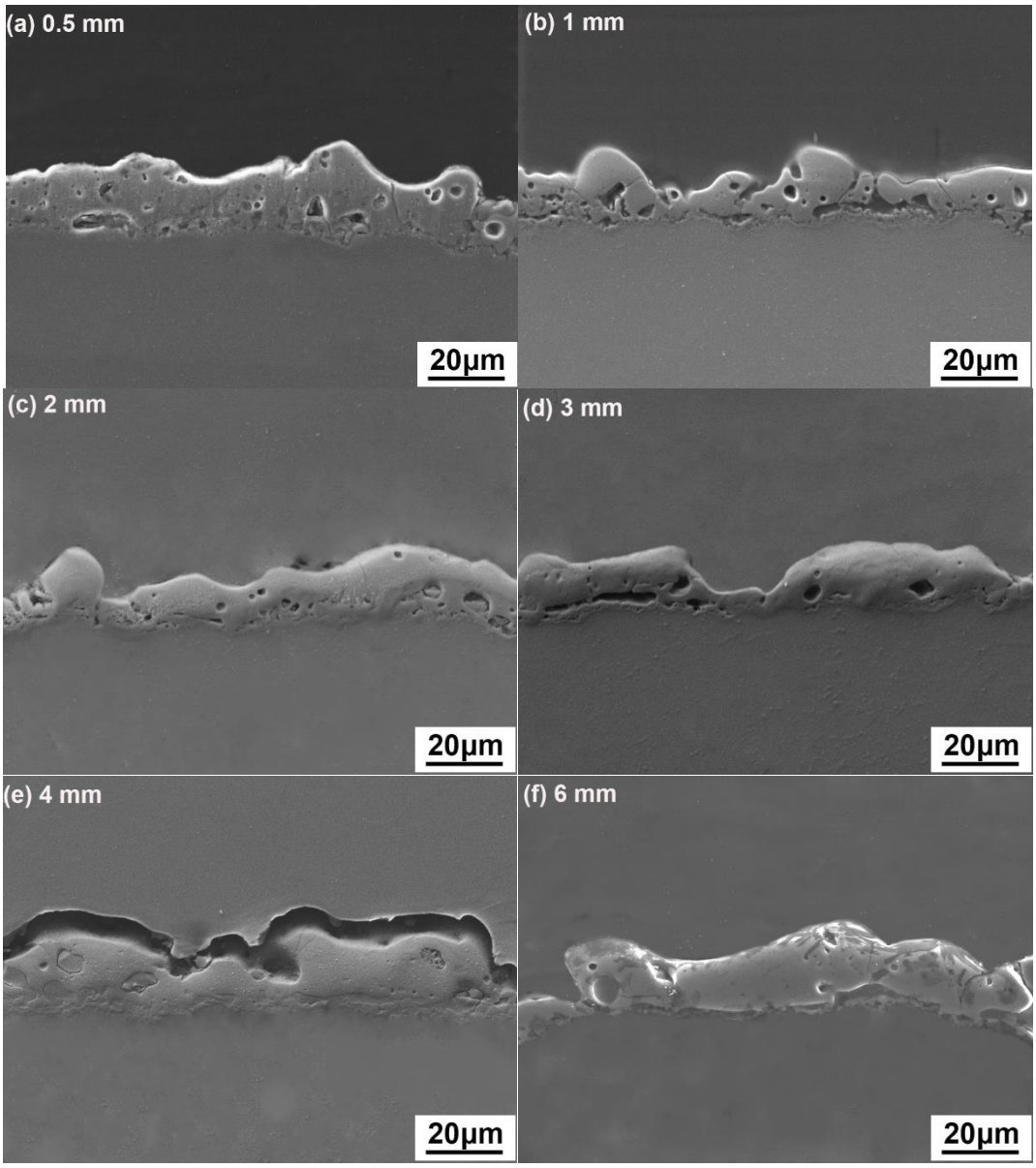

Fig.9 SEM morphologies of the polished cross-sections from the back edges of the round PEO coatings.

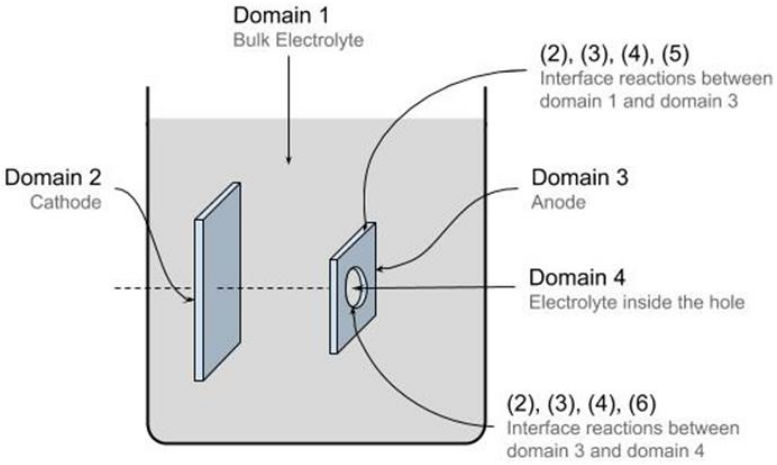

Fig.10 Schematic diagram of the model geometry and the definition of the four domains with the electrochemical reactions taken into account;

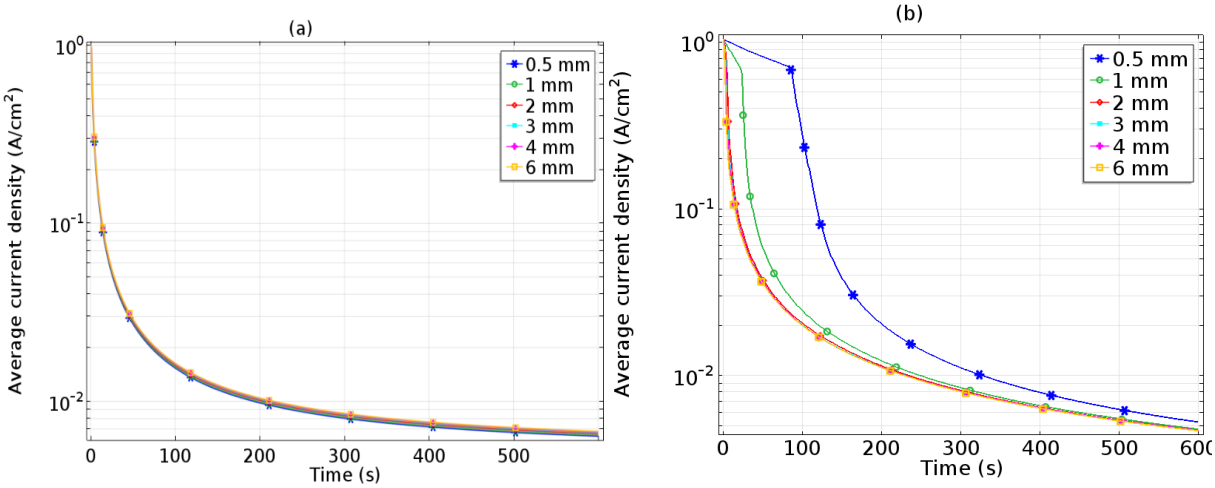

Fig.11 Evolution of average current density on the flat surfaces (a) and round surfaces (b) of anode samples calculated from the modelling in 10 min.

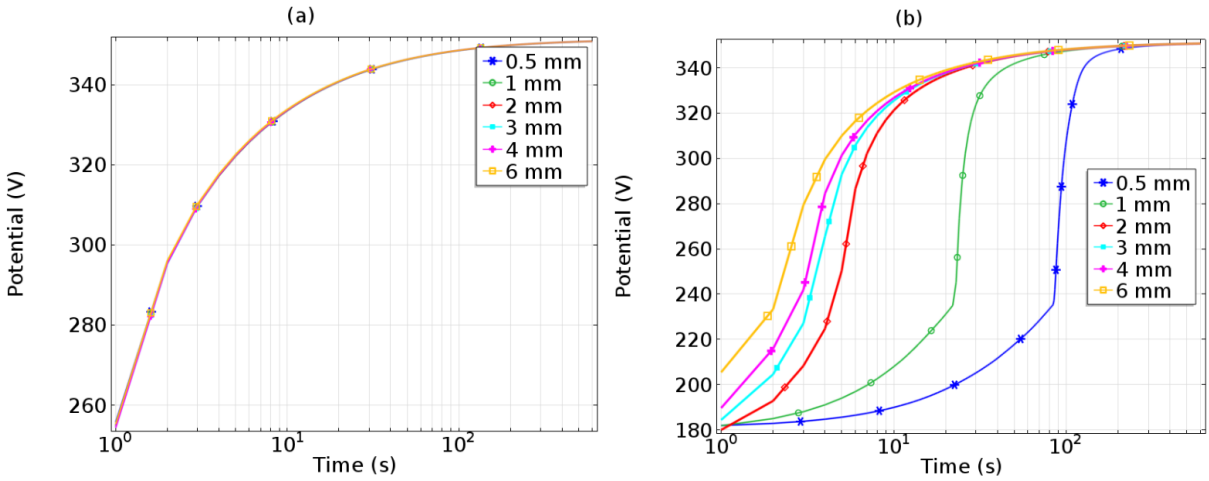

Fig.12 Dependence of potential drop over both flat coatings (a) and round coatings (b) on the PEO processing time for samples with diameters of holes from 0.5 mm to 6 mm.

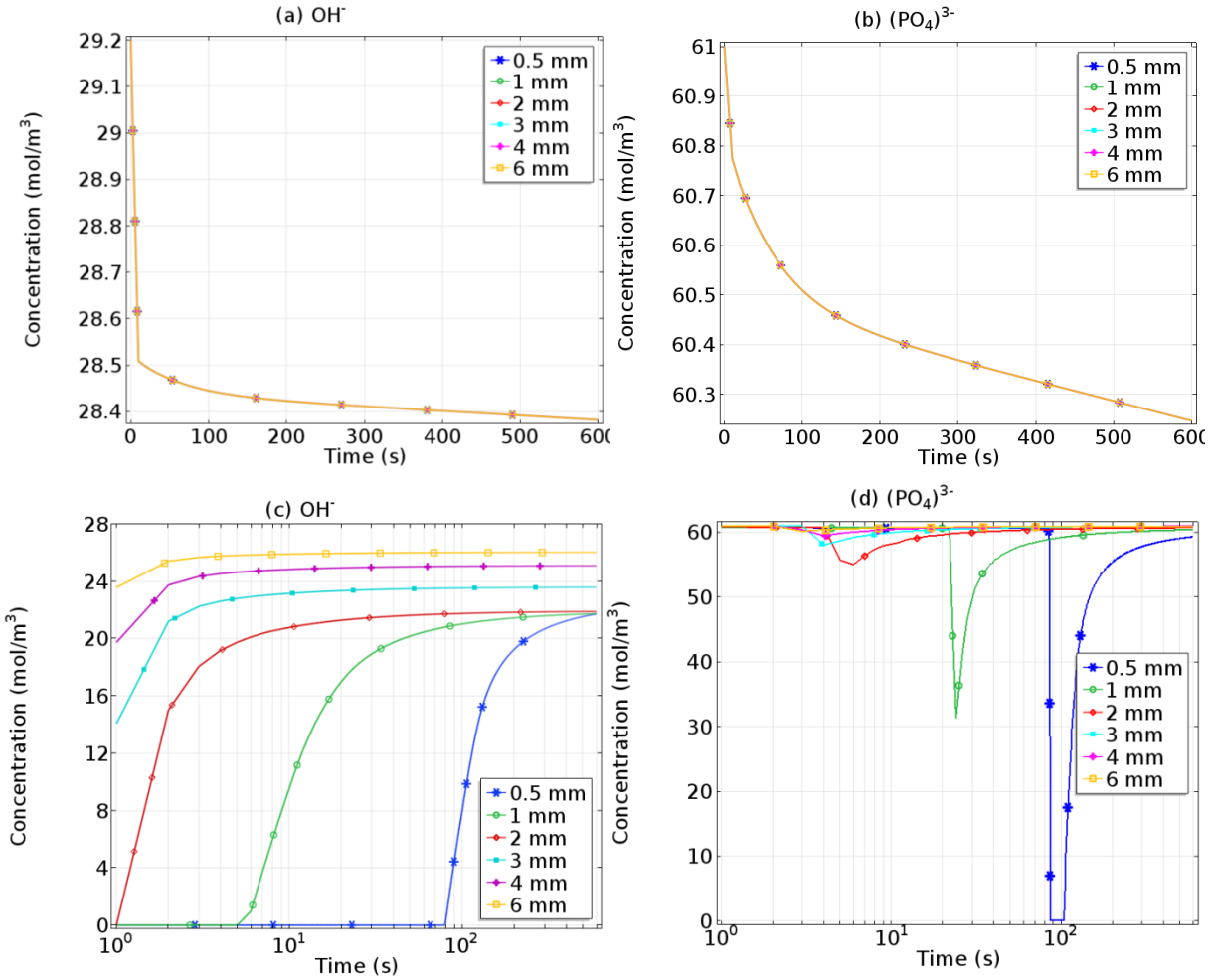

Fig.13 Simulation results of average concentrations of OH^- and PO_4^{3-} both in the bulk electrolyte (a and b) and in the electrolyte inside the holes (c and d) over time.

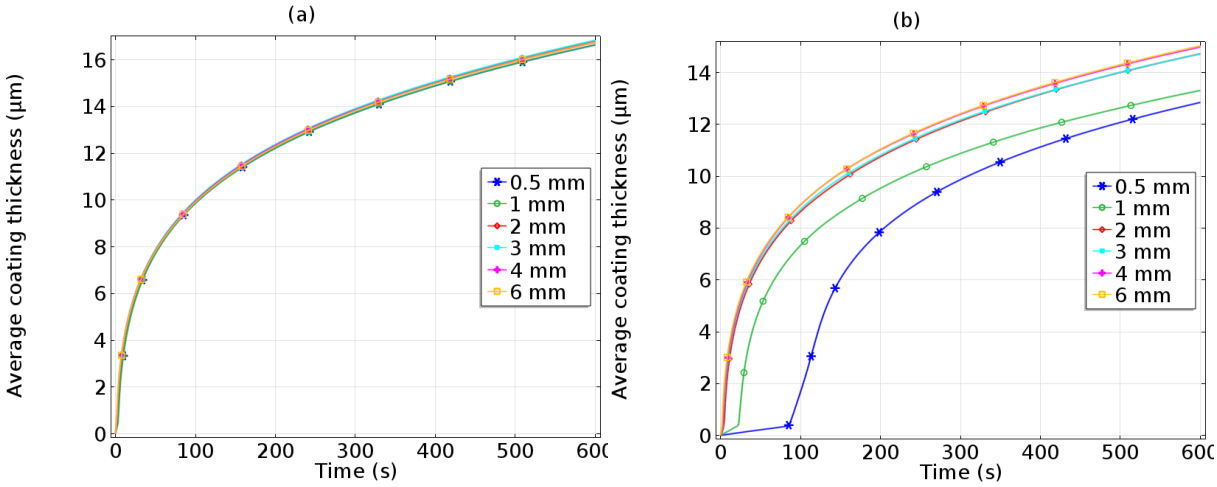

Fig.14 Evolution of average coating thickness on flat surfaces (a) and round surfaces (b) of the samples with diameters of the holes ranging from 0.5 mm to 6 mm.

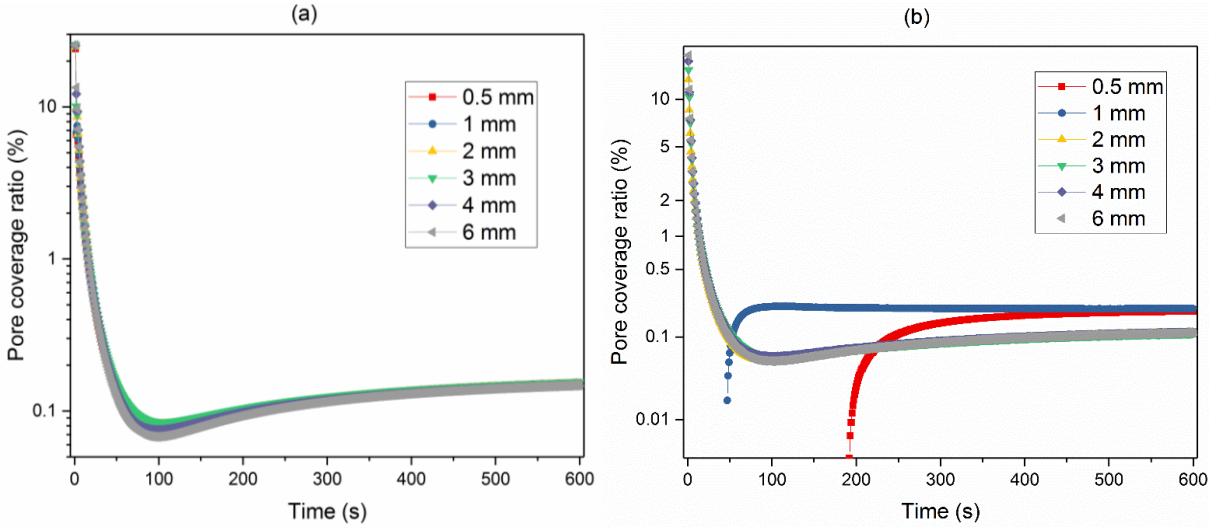

Fig.15 Evolution of pore coverage ratio with time on flat surfaces (a) and round surfaces (b) of samples with diameters of holes ranging from 0.5 mm to 6 mm.

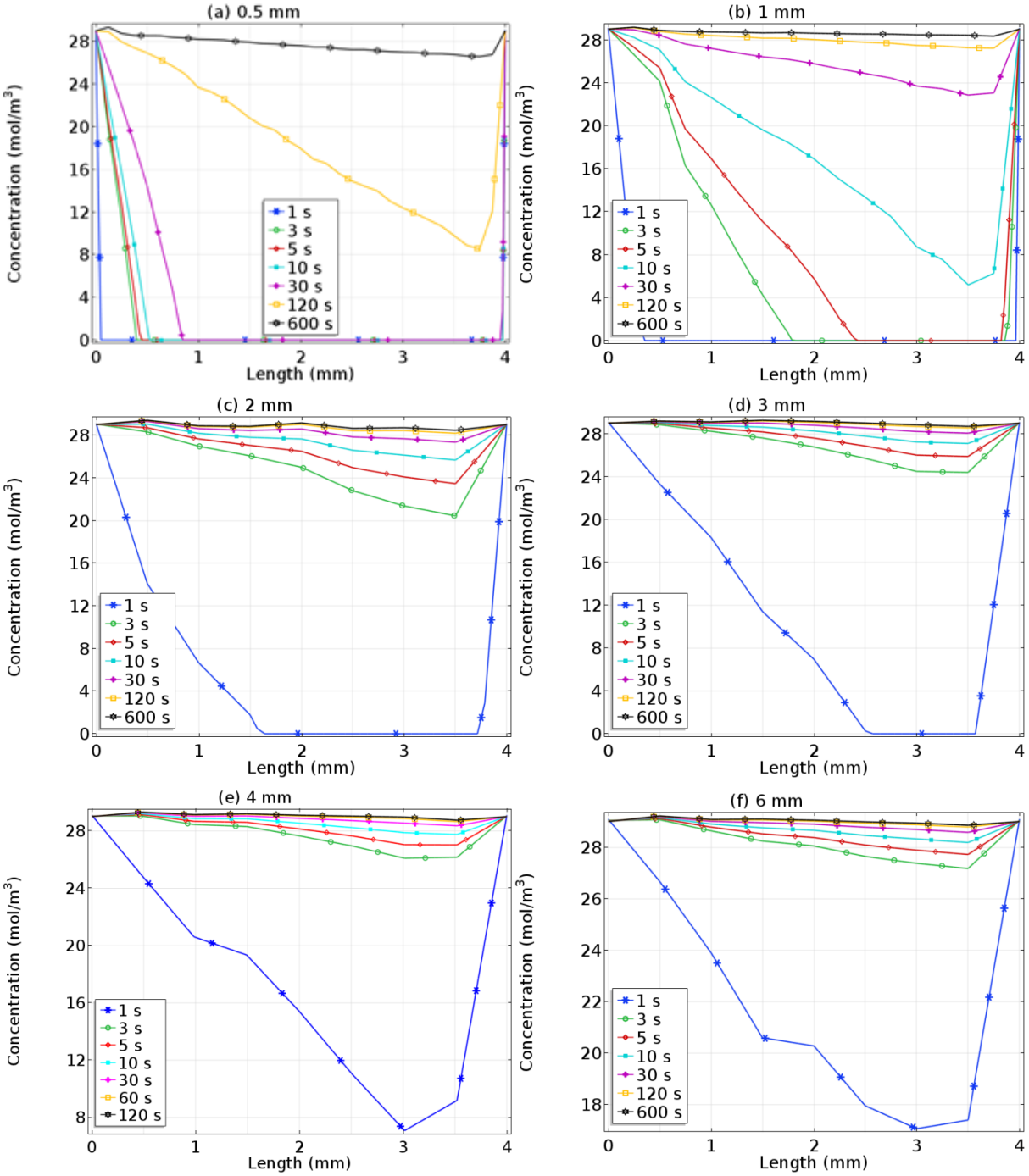

Fig.16 Time dependence of OH^- concentration distribution along the length of round surfaces inside the holes with diameters ranging from 0.5 mm to 6 mm.

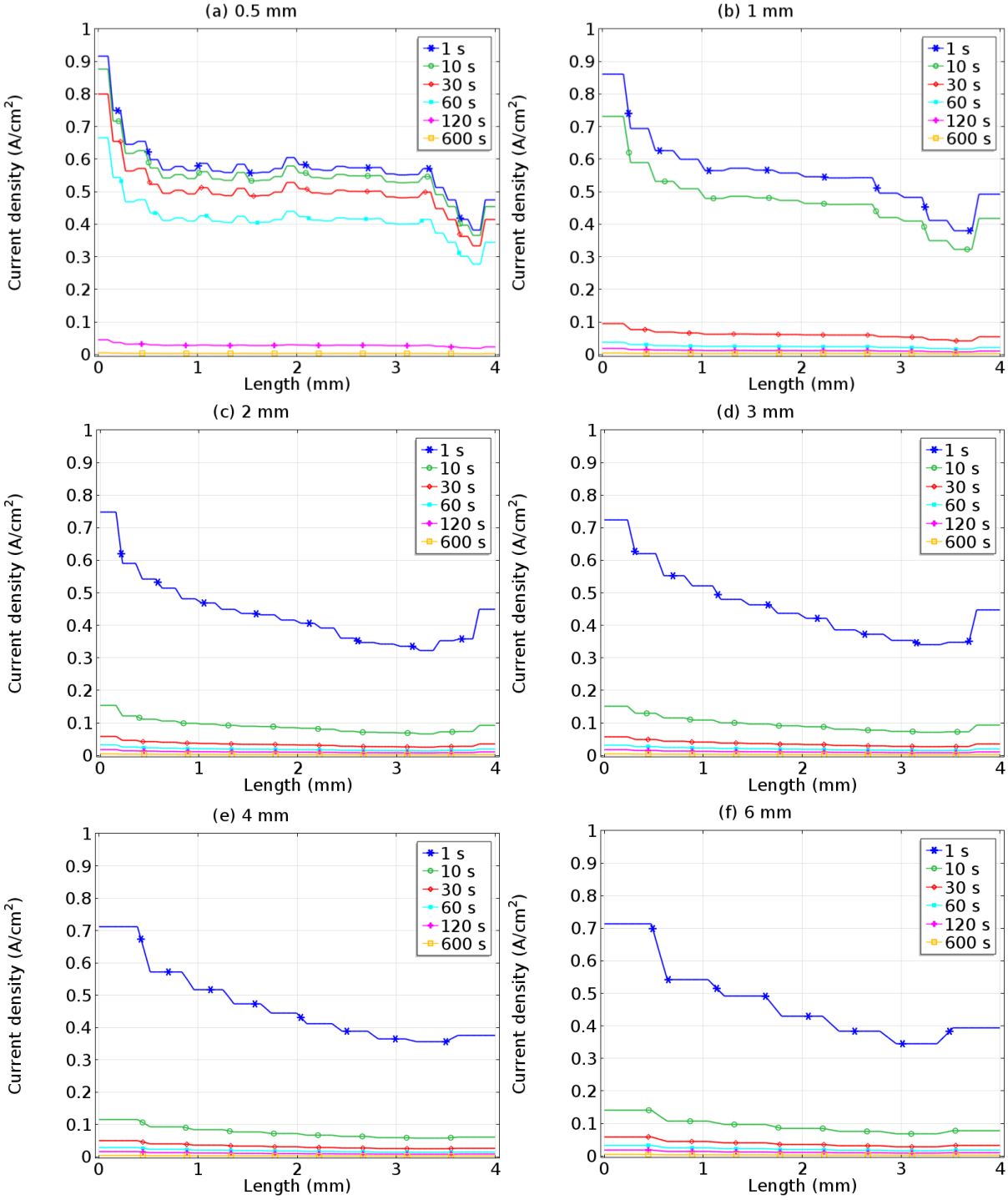

Fig.17 The simulated distribution of current density along the length of the hole from the front side to the back side for each sample with hole diameter from 0.5 mm to 6 mm.

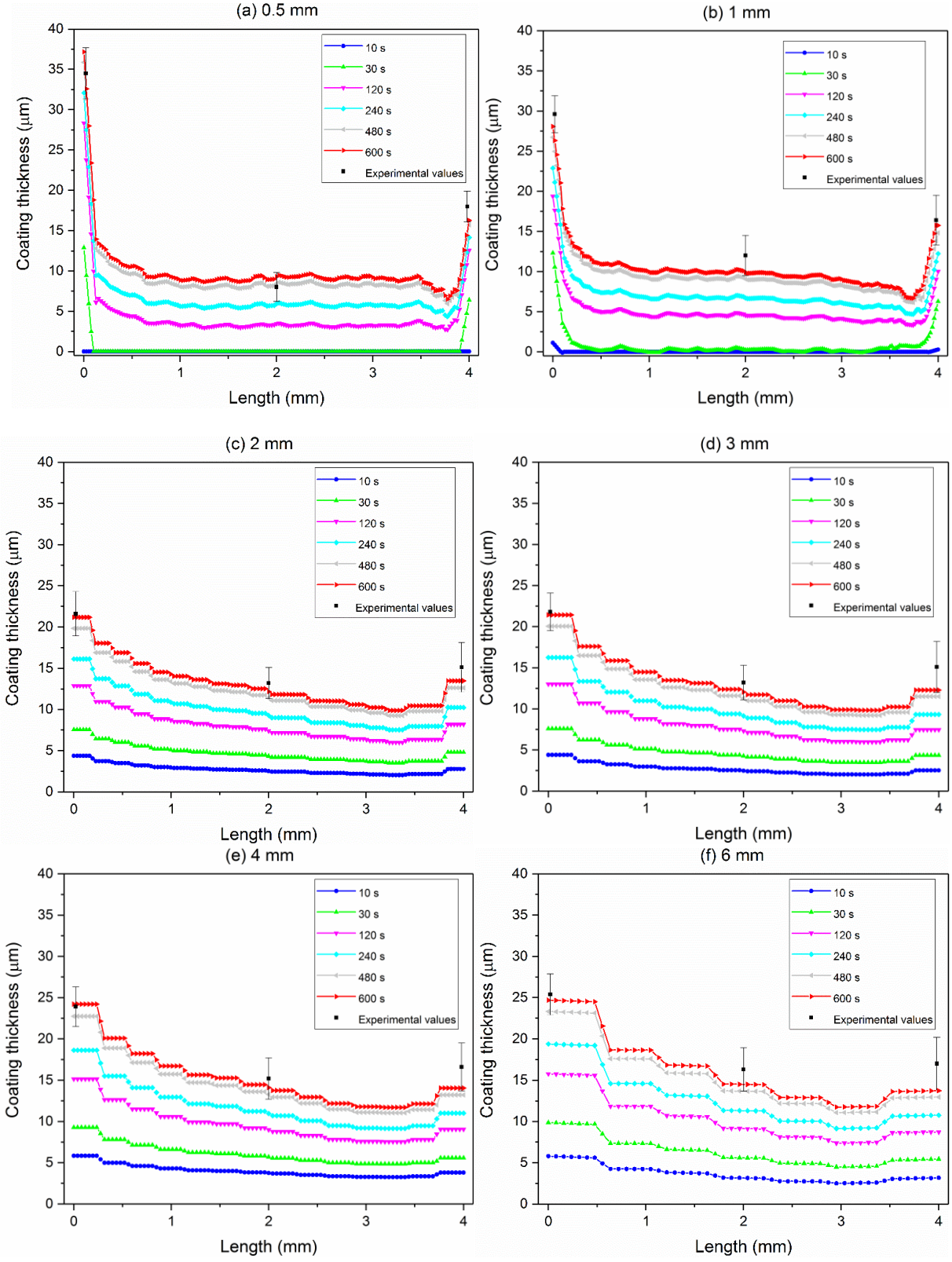

Fig.18 Coating thickness develpoment within 10 min along the length of the hole from the front side to the back side for each sample with hole diameter from 0.5 mm to 6 mm, and the experimental thickness at three locations of each coating after 10 min PEO processing.

Table 1. Diffusion coefficients (D), initial concentrations (C_o) and charge numbers (z) of the species involved in the electrolyte for simulation

Species	D (e-9 m^2/s)	C_0 (mol/m^3)	z	Reference
Mg^{2+}	0.71	0	2	26
PO_4^{3-}	0.37	183	-3	27
OH^-	5.3	29.2	-1	26
H^+	9.3	1e-10	1	26
Na^+	1.3	61	1	26
K^+	2.1	17.8	1	28
O_2	2.4	0.233	0	26

Table 2. Physical input parameters used in the numerical simulation

Physical parameter	Value	Unit
T	283.15	K
U	350	V
σ_{el}	1.4	S/m
j_p	3.0	A/cm^2
A	1.6e-2	A/cm^2
B	122	-
K	7.5e4	1/m
σ_o	2e-4	S/m
σ_p	1.4e-6	S/m
E_a	1.23	V
$M_{Mg3(PO4)2}$	262.9	g/mol
$\rho_{Mg3(PO4)2}$	2.2	g/cm^3
M_{MgO}	40.3	g/mol
ρ_{MgO}	3.58	g/cm^3
M_{MgOH}	58.3	g/mol
ρ_{MgOH}	2.34	g/cm^3
L_0	1e-8	m
w	4 π	-
ρ	1.0	g/cm^3
η	1e-3	Pa·s
p_0	0.1	Pa
$Ksp(_{MgOH})$	5.61e-12	M^3
$Ksp(_{MgPO})$	6.31e-25	M^5